Analyst

CRITICAL REVIEW

Advances in nanowire transistors for biological analysis and cellular investigation

Cite this: *Analyst*, 2014, **139**, 1589

Bor-Ran Li,†[ab] Chiao-Chen Chen,†[ab] U. Rajesh Kumar[ac] and Yit-Tsong Chen*[abc]

Electrical biosensors based on silicon nanowire field-effect transistors (SiNW-FETs) have attracted enormous interest in the biosensing field. SiNW-FETs have proven to be significant and efficient in detecting diverse biomolecular species with the advantages of high probing sensitivity, target selectivity, real-time recording and label-free detection. In recent years, significant advances in biosensors have been achieved, particularly for cellular investigation and biomedical diagnosis. In this critical review, we will report on the latest developments in biosensing with SiNW-FETs and discuss recent advancements in the innovative designs of SiNW-FET devices. This critical review introduces the basic instrumental setup and working principle of SiNW-FETs. Technical approaches that attempted to enhance the detection sensitivity and target selectivity of SiNW-FET sensors are discussed. In terms of applications, we review the recent achievements with SiNW-FET biosensors for the investigations of protein–protein interaction, DNA/RNA/PNA hybridization, virus detection, cellular recording, biological kinetics, and clinical diagnosis. In addition, the novel architecture designs of the SiNW-FET devices are highlighted in studies of live neuron cells, electrophysiological measurements and other signal transduction pathways. Despite these remarkable achievements, certain improvements remain necessary in the device performance and clinical applications of FET-based biosensors; thus, several prospects about the future development of nanowire transistor-based instruments for biosensing employments are discussed at the end of this review.

Received 1st October 2013
Accepted 11th December 2013

DOI: 10.1039/c3an01861j

www.rsc.org/analyst

[a]*Department of Chemistry, National Taiwan University, No. 1, Sec. 4, Roosevelt Road, Taipei 106, Taiwan. E-mail: ytcchem@ntu.edu.tw; Fax: +886 2 3366-8671; Tel: +886 2 3366-8198*

[b]*Institute of Atomic and Molecular Sciences, Academia Sinica, P.O. Box 23-166, Taipei 106, Taiwan*

[c]*Nanoscience and Technology Program, Taiwan International Graduate Program, Academia Sinica, Taipei 115, Taiwan*

† These authors contributed equally to this work.

Bor-Ran Li has been a postdoctoral research fellow under the supervision of Professor Yit-Tsong Chen at the Institute of Atomic and Molecular Sciences, Academia Sinica, Taiwan since December 2009. He received his B.S. (1999) and M.Sc. (2001) degree from the Department of Applied Chemistry, National Chiao-Tung University in Taiwan. Following this, he serviced as a national compulsory research assistant at Institute of Biomedical Sciences, Academia Sinica (2001–2005), and then moved to Scotland and obtained his Ph.D. degree in chemistry/biochemistry from Edinburgh University, UK (2009). His current interests are focused on the design and fabrication of silicon nanowire field-effect transistors for clinical diagnosis and biological research.

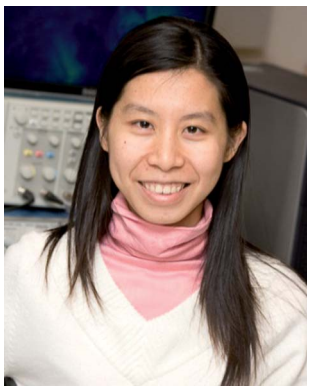

Chiao-Chen Chen received her B.S. (2002) and M.Sc. (2004) degree from the Department of Chemistry at National Taiwan Normal University in Taiwan. After graduation, she worked as a research assistant in the Department of Chemistry at National Cheng Kung University, Taiwan (2005–2006). She then moved to the United States where she obtained her Ph.D. degree in analytical chemistry from the Department of Chemistry, Indiana University Bloomington, USA (2007–2012). Currently, she works as a postdoctoral researcher in Professor Yit-Tsong Chen's group at National Taiwan University. Her research interests are in fundamental study and advanced applications of 2D nanomaterial-based field-effect transistors for energy conversion and biosensing.

1 Introduction

A biosensor is a device that can convert biochemical events into quantifiable electronic signals and is defined by IUPAC as a self-contained integrated device that allows the analytical detection of the specific biochemical occurrence in direct spatial contact with a transduction element.[1,2] A biosensor is an important tool for qualitative and quantitative analyses of biochemical circumstances in biomedical diagnosis and cellular investigations. Although research on biosensors has lasted more than a half century, the development of novel biosensing techniques remains in great demand for advancements in medical diagnosis,[3] toxicity testing,[4] chemical analysis,[5] food industry,[6] and many other fields.[7] Specifically, to design a well-functionalized biosensor to monitor living systems, several essential features are necessary in the device fabrication, such as robustness, ultra-sensitivity, target specificity, rapid response, and real-time recording of the sensorial instrument for biosensing investigations.

Research on nanomaterials in the past two decades has experienced an explosive growth in the study of nanoscale objects, such as quantum dots, nanoparticles, nanowires (NWs), nanotube (NTs), and nanoscale films.[8–14] These newly developed nanomaterials have been tailored to construct novel, functionalized devices to reinvigorate traditional existing techniques. For example, the development of one-dimensional (1D) NW/NT field-effect transistors (FETs) as an extension of traditional two-dimensional (2D) metal-oxide-semiconductor field-effect transistors (MOS-FETs) has demonstrated their exceptional advantages and outstanding performance in many innovative applications.[15–18] The use of these NW/NT-FETs as biosensors has recently attracted tremendous interest in biological studies. Because the sizes of biological macromolecules (*e.g.*, proteins and nucleic acids) are comparable to NWs/NTs, the interaction between biomolecules and NWs/NTs is expected to induce a significant change in the physicochemical properties on the NW/NT-FET surface. Moreover, a NW/NT has a large surface-to-volume ratio, which permits a small variation in the local charges on the NW/NT-FET surface, resulting in a significant conductance change inside the NW/NT-FET due to an electric-field effect. NW/NT-FETs modified with selected receptor molecules (also called probe molecules) can be used as biosensors to detect specific targets in real-time with label-free, sensitive and selective sensing.[19–23] Over the past decade, many types of semiconducting materials, such as silicon nanowires (SiNWs),[19,22,24] carbon materials (*e.g.*, carbon nanotubes (CNTs) and graphene)[25–27] and metal-oxide nanowires (*e.g.*, In_2O_3-NWs and ZnO-NWs),[28,29] have been selected as promising candidates for the development of FET-biosensors.[27]

CNTs, which offer high electron mobility and ultra-small diameters, are one of the most attractive 1D nanomaterials for the fabrication of FETs. Over the past decade, single-wall carbon nanotube field-effect transistors (SWCNT-FETs) have been applied extensively for biosensing detections.[30–38] With appropriate surface modification of receptors, such as deoxyribonucleic acid (DNA), ribonucleic acid (RNA), proteins, antibodies, and aptamers, SWCNT-FETs can serve as ultra-sensitive biosensors for detecting various biomolecular and cellular events. For example, Pui *et al.* have employed SWCNT-network (SWCNT-net) FETs for the extracellular detection of the

U. Rajesh Kumar obtained his Bachelor of Technology in Biotechnology from Anna University (2008) and Master of Technology in Nanotechnology from Indian Institute of Technology Roorkee (2010). Later he joined the Nanoscale Materials and Bio-analytical Chemistry lab through Taiwan International Graduate Program (TIGP) offered by Academia Sinica to pursue his doctorate in Nanoscience and Nanotechnology under the supervision of Professor Yit-Tsong Chen. His current research interests are the fabrication of field-effect transistors using 2D layered materials and biosensing.

Yit-Tsong Chen is a professor in the Chemistry Department of National Taiwan University. He is also an adjunct Research Fellow at the Institute of Atomic and Molecular Sciences, Academia Sinica in Taiwan. He joined the faculties in 1991 after receiving his B.S. degree from National Taiwan University (1980) and Ph.D. degree from the University of Chicago (1988) and having postdoctoral research training at MIT (1989–1991). In his early research career, he was interested in studies of the superfine structures, vibrational dynamics, and Rydberg states of fundamental molecules using a variety of nonlinear laser optics. In the late 1990s, fascinated by the nanoscale world, he shifted part of his research to catalytic growth and spectroscopic characterization of nanoparticles and nanowires. His current interests are focused on applying field-effect transistors, scanning probe microscopy and optical imaging microscopy as biosensors to study protein–protein interactions, extracellular ionic fluctuation, cellular exo-endocytosis and neuron–neuron interactions.

cellular bioelectricity of cardiomyocytes.[39] In their study, SWCNT-net FETs were constructed with a facile drop-casting method to form a ring shape SWCNT-net (~4 mm in diameter) on a glass slide, followed by the fabrication of source and drain electrodes with silver conducting paint. These SWCNT-net FETs enable non-invasive bioelectrical recording of cardiomyocytes, providing a promising platform for the investigation of cellular responses before and after drug treatment. However, unlike SiNW-FETs, the surface of carbon nanotubes lacks a native insulating layer; in addition, the contact of a CNT with nickel (Ni) or titanium (Ti) electrodes is not a perfect ohmic contact.[40,41] Consequently, the working principle of the CNT-FET biosensors does not resort to a pure field-effect; instead, the recoded signals could be induced by field effect,[31] electron transfer,[31] and Schottky barrier variation.[42] Like CNT belonging to the allotropes of carbon, graphene, a two-dimensional nanomaterial composed of sp^2 bonded carbon atoms arranged in a honeycomb crystal structure, has been considered as a promising candidate for advanced applications in biosensing.[37,43–50] However, several challenges for constructing high performance graphene-FETs still remain. In particular, due to the lack of an energy gap in graphene, the graphene-based transistors were hampered to possess high on/off current ratios.[51] In addition, a better control of contact resistance that exists in the interface between graphene and the metal electrodes plays an important role in the integration of graphene-based electronics.[52,53]

Among the 1D NW/NT-FETs, SiNW-FETs have attracted significant attention by taking advantage of the device design and lithographic fabrication from the mature silicon industry. "Top-down" and "bottom-up" are two major fabrication techniques in the preparation of SiNW-FETs. The "top-down" SiNW-FETs are fabricated from silicon-on-insulator (SOI) wafers[54] using lithographic processes combined with physical etching (*e.g.*, electron-beam technique) to define the SiNW patterns. In contrast, the preparation of "bottom-up" SiNW-FETs starts with the growth of SiNWs, normally in a chemical vapor deposition (CVD) reaction. Therefore, the n-/p-type semiconducting property, doping density and charge mobility in the SiNWs can be designed in advance. The synthesized single-crystalline SiNWs will then be assembled into designated arrays followed by electrode fabrication *via* photolithographic or electron-beam lithographic procedures to construct functionalized SiNW-FET devices.[55,56]

In the biological studies that use SiNW-FETs as biosensors for molecular recognition and cellular recording, SiNW-FETs have thus far been successfully employed for the highly sensitive detection of proteins,[24] DNA,[57,58] RNA,[59] cancer markers,[60] viruses[61,62] and other biochemical species.[22,63,64] SiNW-FETs have also been used to monitor the electrical response from live neurons[65] and to detect the exocytotic release from living cells under pharmacological stimulations.[66,67] In addition, the achievement in the successful construction of three-dimensional (3D) nano-FET probes for single cell recording demonstrates that the SiNW-FET biosensors are a promising platform for versatile investigations of living biological systems.[68]

This review summarizes the recent advances in transistor-based biosensors with emphasis on SiNW-FETs. We start with a brief description about the working principle of a SiNW-FET biosensor, followed by detailed discussions on the topics concerning the apparatus of a SiNW-FET system and the biological applications from the employment of novel SiNW-FET designs. Novel architecture designs of SiNW-FET devices are highlighted in studies of live neuron cells, electrophysiological measurements, and other signal transduction pathways. Then, challenges that may be encountered in the future with FET-based measurements are discussed. Finally, an overview of the importance of applying NW-FET biosensors in biological analysis and cellular investigation is presented.

2 Working principle and experimental setup

As illustrated in Fig. 1A, a NW-based FET device is composed of a semiconductor channel and source, drain and gate electrodes, all of which are located on a substrate (commonly a Si wafer) with an insulating (dielectric) surface layer.[69] The source and drain electrodes communicate with each other through the semiconductive channel, while the gate electrode is used to modulate the channel conductance *via* an applied electrical potential. For a SiNW-FET to be used in the sensing modality, the semiconductive channel configured by SiNW(s) between the source and drain electrodes acts as an effective sensing element of the device, whose sensitivity is attributed to its sensible response to the variation of an external electric field (correspondingly, an electrical potential[70]) on the SiNW surface. In biosensing applications, the SiNW-FET device is mostly immersed in a physiological buffer that is commonly utilized to maintain the activity of biological systems (*e.g.*, biomolecules, cells, tissues, *etc.*); by the same token, a silica sheath (a natural insulator) on the SiNW and the coating of an insulating layer (*e.g.*, silicon nitride, aluminum oxide, *etc.*) on the metal electrodes are necessary to prevent electrical leakage from the SiNW-FET to the electrolytic buffer. For target selectivity, the SiNW-FET can be functionalized by modifying selected receptor molecules on the SiNW surface to bind specific target analytes. The target–receptor binding will render a depletion or accumulation of charge carriers inside the SiNW-FET, thus modulating the source–drain current (I_{sd}), which can then be acquired as a signal with a lock-in amplifier system. The variation of I_{sd} depends on the interaction potential ($V(r)|_{r=r_{bs}}$) of the bound target molecules that are imposed on the sensing SiNW, the distance (r_{bs}) of the target–receptor binding site to the SiNW surface, and the electric field screening effect due to the environmental electrolytic solution, as will be discussed later. To maintain the performance stability of a biosensing system, an Ag/AgCl reference electrode is immersed in the sample solution and is maintained at ground potential to reduce electrical noise. Alternatively, the Ag/AgCl electrode can also be used as a solution gate controller in electrical measurements with the gate voltage (V_g) being supplied by a data acquisition (DAQ) system. Fig. 1B demonstrates the changes of the electrical conductance

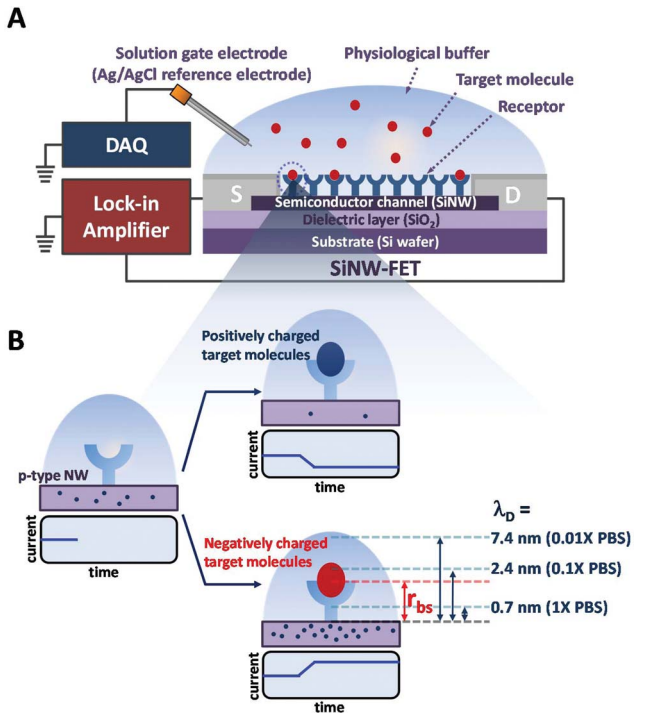

Fig. 1 Schematic illustrations of an experimental setup and the working principle of a SiNW-FET biosensor. (A) A SiNW-FET contains a semiconductive channel, composed of a single SiNW or a bunch of SiNWs, which is electrically connected between source and drain electrodes located on a Si wafer. The electrical measurements of a SiNW-FET are conducted with a lock-in amplifier in the presence of a Ag/AgCl reference electrode, serving as a solution gate by inserting it directly into the buffer solution. The solution gate voltage is supplied by a data acquisition (DAQ) system. (B) Receptor molecules are immobilized on the SiNW(s) to recognize specific targets with a SiNW-FET biosensor. When positively charged targets bind on a p-type SiNW-FET, a depletion of charge carriers (holes) in the SiNW occurs, leading to a decrease in the electrical conductance. Conversely, the binding of negatively charged targets causes an accumulation of charge carriers to induce an increase in conductance. This polarity of the conductance change is reversed for an n-type SiNW-FET. The calculated Debye–Hückel lengths of λ_D = 0.7 nm for 1× PBS, λ_D = 2.4 nm for 0.1× PBS, and λ_D = 7.4 nm for 0.01× PBS solutions are also indicated.

in a p-type SiNW-FET during the target–receptor binding.[69] The charge carriers in the p-type SiNW-FET are dominated by a surplus of holes, which are depleted to reduce I_{sd} when positively charged targets are captured by the receptors on the SiNW surface. Likewise, the accumulation of holes to increase I_{sd} results from binding negatively charged targets.

3 Electrical measurement and device performance

In biosensing measurements, the detection sensitivity, performance stability and device reliability of a SiNW-FET biosensor should be emphasized. Several key factors concerning the electrochemical principles and device designs that are involved in the operational processes must be considered, such as the Debye–Hückel screening effect, device reusability, data normalizations and sensitivity enhancement.

3.1 The Debye–Hückel screening effect

The sensing mechanism of an FET sensor is based on the conductance change in the active sensing channel of the FET device due to the interfering electric field/potential imposed by the charged targets bound on the sensing channel. In biosensing measurements, the FET device is mainly dipped in an aqueous electrolytic environment of physiological buffer, *e.g.*, phosphate buffered saline (1× PBS), consisting of 137 mM NaCl, 2.7 mM KCl, 10 mM Na_2HPO_4, and 2 mM KH_2PO_4 in NaOH at pH 7.4. Because of the electrolytic medium, the interaction potential ($V(r)|_{r=r_{bs}}$) toward the FET sensing channel, exerted from the captured target charges, is attenuated according to the Debye–Hückel screening effect:

$$V(r)|_{r=r_{bs}} = V(r_{bs})e^{\frac{-r_{bs}}{\lambda_D}}, \quad (1)$$

where r_{bs} is the distance of the target–receptor binding site to the SiNW surface and λ_D, the so-called Debye–Hückel length,[71,72] is defined as

$$\lambda_D = \sqrt{\frac{\varepsilon_0 \varepsilon_r k_B T}{2N_A e^2 I}}, \quad (2)$$

where ε_0 represents the vacuum permittivity, ε_r is the relative permittivity of the medium, k_B is Boltzmann's constant, T represents the absolute temperature, N_A is Avogadro's number, and e represents the elementary charge. The ionic strength (I) of the surrounding buffer solution can be calculated from

$$I = \frac{1}{2}\sum_{i=1}^{n} C_i Z_i^2, \quad (3)$$

where C_i is the molar concentration (M, mol L^{-1}) of the ion i, Z_i is the charge number of that ion, and the sum is taken over all the ions in the buffer solution. Governed by eqn (2), a buffer solution with a higher ionic strength (*e.g.*, high salt buffer) has a shorter λ_D, thus causing a more severe screening effect on the FET-based sensing measurements. For example, λ_D = 0.7 nm for 1× PBS, λ_D = 2.4 nm for 0.1× PBS, and λ_D = 7.4 nm for 0.01× PBS solutions, as illustrated in Fig. 1B.

3.2 Reusable device system

When using SiNW-FETs to detect a specific target, the SiNW surface must be modified with selected receptors before the detection. Although the strong binding affinity between the target and receptor (such as an antigen and antibody) allows the receptor-modified SiNW-FET to serve as an extremely sensitive gadget, it is difficult to remove the target–receptor complex from the surface of the SiNW after detection, meaning that a SiNW-FET can only be used for a single measurement. Furthermore, the receptors immobilized on the SiNW-FET for biomedical diagnosis are normally proteins, DNA, RNA or antibodies, which are unstable, easily contaminated biomacromolecules and are inappropriate for reuse in long-term analyses. To solve this problem, several reversible surface

modification methods have been recently developed to produce reusable SiNW-FET devices. As schematically illustrated in Fig. 2, two well-known protein trapping systems that are widely used in protein purifications, *i.e.*, the glutathione (GSH)/glutathione *S*-transferase (GST)-tag[24,73] and Ni^{2+}/hexahistidine (His_6)-tag[74–76] systems and a cleavable disulfide bond (S–S)[21,62] technique were adopted to serve as the reversible methods of surface modification on the SiNWs, which allows a SiNW-FET to be used repeatedly for many cycles of sensing measurements. Because the "root" molecules (*i.e.*, the GSH, Ni^{2+}, and thio-group for the three methods presented in Fig. 2) were fixed firmly on the SiNW surface by chemical bonding, without washing-out vulnerably in the repeated cycles of sensing measurements, the number of immobilized receptors can remain the same in consecutive detections, allowing the reusable, calibratable SiNW-FET devices to be used for quantitative analysis.

3.3 Response signal calibration

Although NW-FETs are one of the most promising platforms for biosensing, the device-to-device variation in performance parameters for different batches of production (especially *via* the bottom-up fabrication) remains inevitable. However, a metric system can be established to calibrate the current/conductance changes measured with different NW-FET devices. As depicted in Fig. 3A, the calibration can be realized by converting the measured absolute current response (ΔI_{sd}) due to the target–receptor binding to the change in gate voltage (termed as the calibrated response and represented by ΔV_g^{cal}) according to the I_{sd}–V_g transfer curve of the NW-FET device used.[77] As illustrated in Fig. 3B–D, a comparison of the absolute responses (ΔI_{sd}), normalized response ($\Delta I_{sd}/I_0$), and calibrated response (ΔV_g^{cal}) measured with various NW-FET devices clearly indicates that the coefficient of variation (CV) is reduced from 59% in ΔI_{sd} to 25% in $\Delta I_{sd}/I_0$ and finally to 16% in ΔV_g^{cal}, confirming the effective suppression of the device-to-device variation through an appropriate calibration procedure.[77]

3.4 Detection sensitivity enhancement

In late developments using SiNW-FETs as a sensorial tool for molecular recognition, several efforts have been made to improve the detection sensitivity of these devices.[78] Aside from other studies, we describe three recent advancements in SiNW-FETs for detection-sensitivity enhancement in which these FET devices were used in their sensing modality.

3.4.1 Sensing in the subthreshold regime. Recently, Gao *et al.* reported that the sensitivity of the SiNW-FET sensors can be enhanced exponentially when electrical measurements are conducted in the subthreshold regime of a transfer curve.[79] This sensitivity enhancement stems from the fact that the gating effect of target molecules in the subthreshold regime modulates the conductance inside the SiNW most effectively because of the reduced screening of the charge carriers in the SiNW. To be more explicit, it is the relative magnitude between the carrier screening length (λ_{Si}) and the SiNW radius (R) that determines the effectiveness of the gating effect induced by the target molecules bound on a SiNW-FET, of which the SiNW radius (R) is constant; however, the magnitude of λ_{Si} depends on the doping concentration of the SiNW. For a highly doped regime, λ_{Si} is much smaller than R due to the screening by the carriers; the sensing of the SiNW-FET works in a linear regime, where the device conductance varies linearly with V_g. However, the gating effect due to the surface charges induced by target molecules cannot modulate the entire cross-section of a SiNW, thus limiting the detection sensitivity of a SiNW-FET. In contrast, when a SiNW-FET works in the depletion (subthreshold) regime, the low carrier concentration results in a reduced screening effect ($\lambda_{Si} \gg R$). Consequently, the gating effect caused by charged targets can reach the entire cross-section of the SiNW and induce an exponential response in the variation of device conductance. Accordingly, a SiNW-FET biosensor should work in the subthreshold regime ($\lambda_{Si} \gg R$) to increase its detection sensitivity by extending the gating effect toward the entire SiNW. Furthermore, a SiNW-FET can only fully utilize the high surface-to-volume ratio of the NWs to effectively achieve optimal detection sensitivity in this subthreshold regime.

3.4.2 Frequency-domain measurement. Recently, Zheng *et al.* demonstrated protein detection using a SiNW-FET with a new methodology based on a frequency (f)-domain electrical measurement.[80] In this study, the power spectral density of voltage from a current-biased SiNW-FET was investigated by demonstrating the $1/f$-dependence in the frequency domain for the measurements of target–receptor binding. As a representative test in their study of scanning the $1/f$-dependence in the frequency domain, an antibody-modified SiNW-FET was employed to detect the targeted antigen with specific or non-specific binding to the antibody receptor. In the presence of the targeted antigen that could be recognized specifically by the antibody-modified SiNW-FET, the $1/f$ spectrum exhibited a Lorentzian spectral shape with a characteristic frequency of several kHz, which is regarded as being associated with the antigen–antibody binding–unbinding rates. Two sources ascribed to explaining the observed Lorentzian shapes in the observed $1/f$ noise spectra include (a) the equivalent gate voltage noise from the binding–unbinding of the individual antigen to antibody receptors and (b) the additional thermal (Johnson) noise associated with the antibody and bound antigen layers. In this method, the spectral shapes of the frequency spectra were utilized to monitor the binding events and to further determine the detection limit by the $1/f$ measurement. Facilitated by this new methodology of frequency-domain measurement, the detection sensitivity was claimed to increase by more than 10-fold compared with conventional time-domain measurements.

3.4.3 Selective surface modification. Because SiNWs are normally covered with a thin silica sheath, resulting from the oxidation of their surfaces upon exposure to air, these NWs have no chemical specificity toward particular analytes. In biosensing detections with SiNW-FETs, the SiNW surface can be modified with selected receptor molecules that allow the SiNW-FETs to achieve target selectivity and high detection sensitivity.[19,81,82] One economical, efficient and commonly used SiNW-FET surface-modification method is to use a chemical linker, *e.g.*, 3-aminopropyltrimethoxysilane (APTMS), which

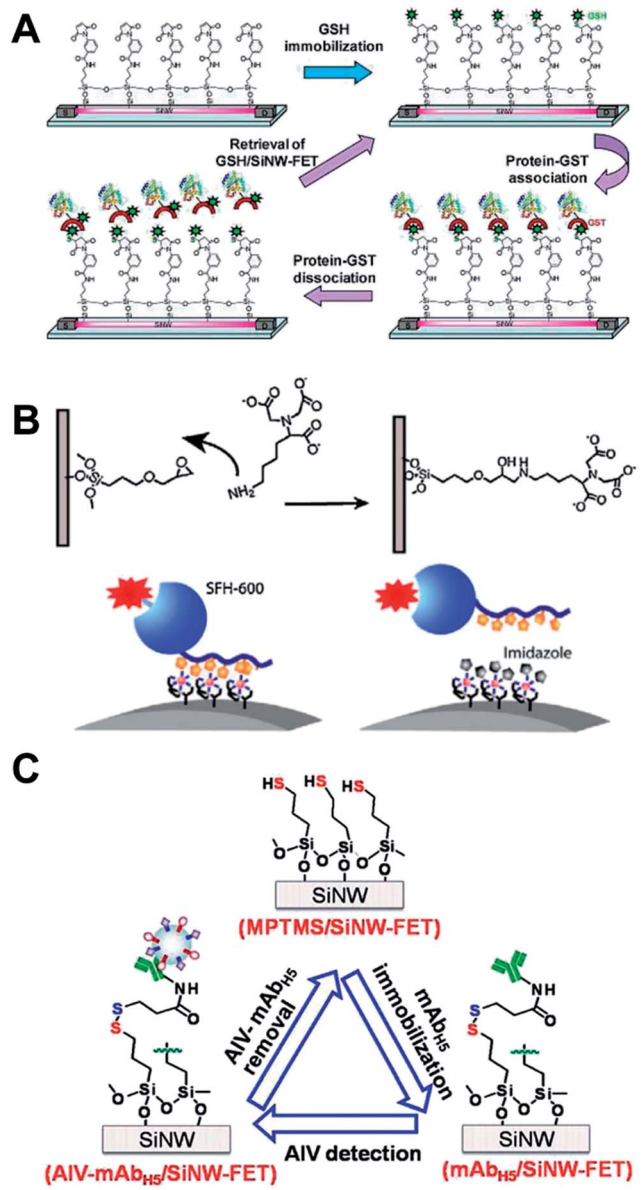

Fig. 2 Schematic representations of creating a reusable SiNW-FET system with three reversible surface-modification methods. (A) A SiNW-FET is first immobilized with GSH to form a GSH/SiNW-FET device, which can then be used to bind GST-fusion proteins. At the end of each measurement, the captured protein–GSTs are eluted with a high concentration of GSH solution (≥1 mM) to return the device to its original state, making the GSH/SiNW-FET a reusable biosensor. (B) A reusable FET sensor is formed by surface modification of (3-glycidyloxypropyl) trimethoxysilane and *N*-(5-amino-1-carboxypentyl) iminodiacetic acid, which is ready to bind His_6-tagged proteins in the presence of Ni^{2+}. After the binding, the His_6-tagged proteins can be removed by flushing with imidazole or ethylenediaminetetraacetic acid (EDTA). (C) The detection of a virus with a reusable SiNW-FET *via* the cleavage of a disulfide bond. A SiNW-FET is initially modified with mercaptopropyltrimethoxysilane (MPTMS) to form MPTMS/SiNW-FET, followed by immobilizing the receptor (antibody) through a disulfide bond. In biosensing measurements, the antibody captures the targeted virus to form a complex. After detection, the virus–antibody complex on the SiNW-FET can be removed by cleaving the disulfide bond with dithiothreitol (DTT), thus returning the device surface to its original MPTMS/SiNW-FET. Panels (A), (B) and (C) are reprinted with permission from ref. 73, 74 and 62, respectively. Copyright Elsevier, IOP publishing and Wiley-VCH Verlag GmbH & Co. KGaA.

immobilizes the receptor molecule and anchors to the silica sheath of the SiNW at opposite ends of the linker. However, the silica sheath on the SiNW surface is no different from the oxidized layer of a Si wafer, which is usually used as a substrate for the fabrication of the SiNW-FET devices. Upon surface modification, receptor molecules are immobilized over the entire silica surface, covering not only the minute SiNW surface but also the relatively large surrounding substrate area. These types of SiNW-FET devices, which have all area modification (AAM), are denoted AAM SiNW-FETs (as illustrated in Fig. 4A and B). The ratio of the surface area of the SiNW to the area of the surrounding substrate reflects the relative probabilities of these two surfaces coming into contact with an analyte molecule. In biosensing measurements using an AAM SiNW-FET, the ratio of the surface areas of the SiNW and the surrounding substrate is very small (typically on the order of one millionth). This small ratio is undesirable because a large proportion of the target molecules are likely to be captured by the receptors immobilized on the surrounding substrate before arriving at the actual sensing element of a SiNW-FET device; the large proportion of captured molecules consequently jeopardizes the detection sensitivity of the AAM SiNW-FET (Fig. 4A and B).

SiNW-FETs that have selective surface modification (SSM), with receptors modifying only the SiNW surface without contaminating the surrounding substrate, are called SSM SiNW-FETs (Fig. 4A and B). Several approaches that have been used to reduce the modification by receptors on the non-sensing area include photolithography,[71] microcontact printing,[83] electrostatic attraction,[84] dip-pen nanolithography,[85] localized Joule heating,[86] and incomplete chemical etching.[87] However, these methods are more suited to an SOI-based top-down approach. Recently, Li *et al.* also used a bottom-up technique to successfully fabricate SSM SiNW-FETs with the receptors modified on the SiNW sensing surface only.[88] In their approach, the SiNWs were modified with APTMS before photolithographic fabrication of the device. The APTMS molecules modifying the SiNWs survived the harsh photolithographic processes, including photoresist coating, organic solvent washing, and thermal annealing. These SSM SiNW-FETs also exhibited desirable electrical characteristics such as ohmic contact and high transconductance ($g_m = dI_{ds}/dV_g$). In Fig. 4C, a comparative test using biotin-modified SiNW-FETs (called biotin/SiNW-FET) to detect avidin is illustrated. Here, the smaller calibrated response (V_g^{cal}) measured by the AAM system (blue columns) at $C_{avidin} \leq 10$ pM, relative to the SSM system (red columns), arises because in the AAM biotin/SiNW-FET measurements, part of the avidins were captured on the surrounding substrate before arriving at the binding sites on the SiNW. This process resulted in deficient avidins to reach a genuine biotin–avidin equilibrium in the measurements with the AAM system. This deterioration in accuracy is enhanced as C_{avidin} decreases.[88] In the same study, an SSM SiNW-FET demonstrated a substantial improvement over an AAM SiNW-FET, due to superior detection sensitivity, a faster response time and smaller sample requirements, rendering the SSM SiNW-FET a highly sensitive biosensor for molecular recognition.

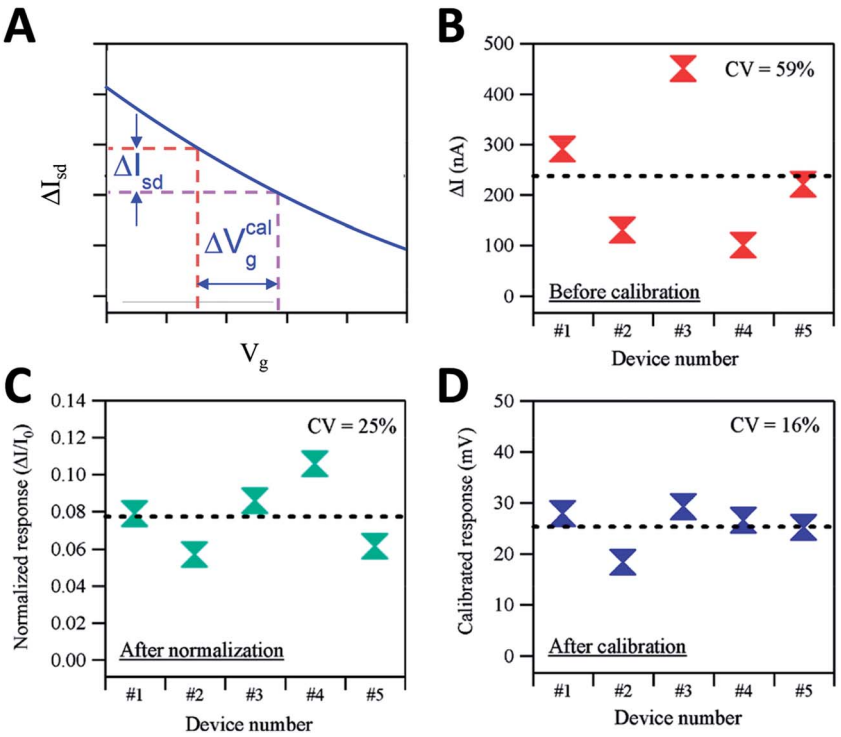

Fig. 3 (A) To avoid device-to-device variation in electrical measurements, the current changes (ΔI_{sd}) can be transformed into corresponding calibrated response changes (ΔV_g^{cal}) with the I_{sd}–V_g transfer curve of the SiNW-FET device used. (B)–(D) A comparison between the absolute electrical signals recorded with an FET device and the normalized signals obtained using different calibration methods. CV represents the coefficient of variation. (B) Measurements of the absolute responses (ΔI_{sd}) recorded from five FET devices before calibration. (C) The same plots taking the same measurements in (B) after conventional normalization. The vertical axis is the normalized response. (D) The same plots after calibration with the gate dependence ($g_m = dI_{ds}/dV_g$). The vertical axis represents the calibrated response (ΔV_g^{cal}). Reprinted with permission from ref. 77. Copyright the American Chemical Society.

4 Biological and cellular applications

4.1 Protein–protein interaction

Understanding how proteins interact with each other is the basis for studying the biological mechanisms behind various physiological activities. In particular, after the human genome was completely sequenced, a myriad of genes were identified but without knowing their functionalities. Therefore, determining how to rapidly understand the interactions of these function-unknown proteins is an important task in the post-gene era. Thus, many approaches have been developed to help biologists draw the map of the protein-network. However, current detection methods rely mainly on various labeling techniques, which usually require a considerable amount of time in performing the labeling procedures. Concurrently, several label-free detection techniques (*e.g.*, surface plasmon resonance imaging (SPRI),[89] atomic force microscopy (AFM),[90] and SiNW-FET/CNT-FET[91,92]) have been applied to study protein–protein interactions. Among them, SiNW-FETs have attracted tremendous attention because of their unique capabilities of providing real-time, highly sensitive, and target selective detections.

In 2001, Cui *et al.* demonstrated the real-time detection of streptavidin with a biotin-modified SiNW-FET biosensor.[19] These authors also demonstrated that the detection limit could be pushed down to ~10 pM, which is much lower than the nanomolar-range detection level obtained using other techniques, such as the stochastic sensing of single molecules.[93] Since the pioneering of this biosensing application, the use of SiNW-FETs has been extended to a broad range of biological investigations. For example, Lin *et al.* demonstrated that a SiNW-FET can be used to study protein–protein interactions; these authors first demonstrated that a calmodulin (CaM)-modified SiNW-FET (called CaM/SiNW-FET) can be used to detect calcium ions (Ca^{2+}). The same CaM/SiNW-FET bio-nano-electronic device was also employed to investigate the CaM–cardiac troponin I interaction and CaM–Ca^{2+} channel coupling.[24] With this bio-nano-electronic design for biosensing measurements, the detailed mechanism of protein–protein interactions can be disclosed from a real-time recording investigation by a SiNW-FET. For instance, the CaM/SiNW-FET was delicately used to prove that a minimum concentration of Ca^{2+} at 1 μM is a prerequisite for the activation of the function of CaM that enables its succeeding interaction with cardiac troponin I. Also, the n-type voltage-gated Ca^{2+} channels expressed by cultured 293 T cells can be recognized specifically by the CaM/SiNW-FET in the presence or absence of Ca^{2+}, revealing that CaM can directly interact with the n-type voltage-gated Ca^{2+} channel.

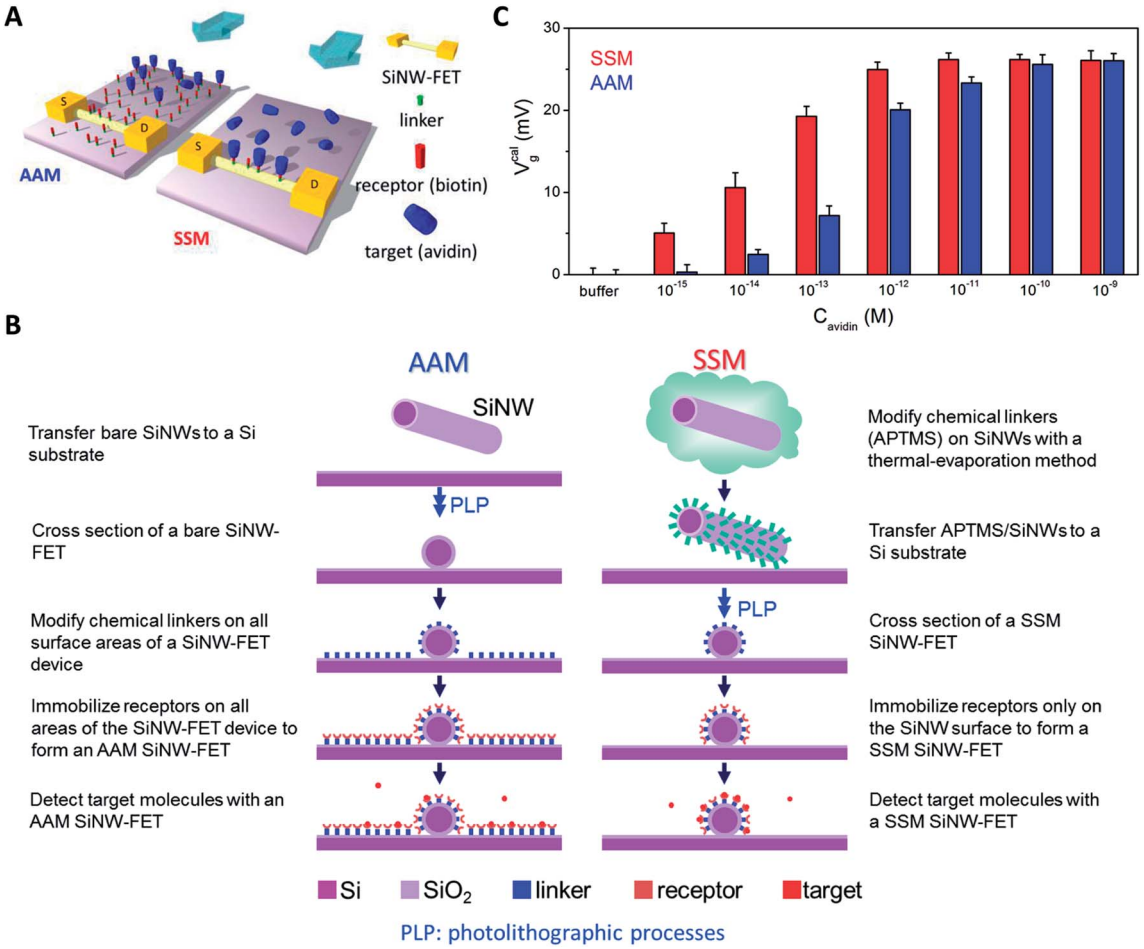

Fig. 4 (A) An illustration depicting the binding competition involved in biomolecular detection by an AAM or an SSM SiNW-FET. (B) Schematic representations of the preparation, fabrication, and biosensing of AAM and SSM SiNW-FETs. (C) A column plot of V_g^{cal}, measured by AAM biotin-SiNW-FET (blue) and SSM biotin-SiNW-FET (red), at different C_{avidin}. The error bars represent the standard deviations of three measurements. Reprinted with permission from ref. 88. Copyright Elsevier.

In the investigation of protein–protein interactions with SiNW-FETs, most of the studies are restricted to a known interacting protein with a pre-selected probe protein. To explore the capability of not only detecting but also analyzing unknown interacting proteins, Lin *et al.* integrated a SiNW-FET with mass spectrometry (MS) for fast screening (by SiNW-FET) and spectral identification (by MS) of the interacting proteins that were captured on the probe protein-modified SiNW-FET.[94] In their study, the GST-tagged CaM proteins were prepared to modify a GSH/SiNW-FET to form a CaM/SiNW-FET. After the cell lysate was passed through the CaM/SiNW-FET, the binding proteins in association with CaM induced a conductance change inside the CaM/SiNW-FET. The bound proteins were then eluted out of the CaM/SiNW-FET (because of the reversible association–dissociation of the GSH/GST pair) and subsequently identified by MS as kinase IIα. In another example with the same SiNW-FET sensing technique, the heat shock protein, the 70 kDa protein 1A/1B (Hsp 70), was identified to be a calneuron I binding protein. These results demonstrate the effectiveness of integrating MS with SiNW-FET for rapidly screening and correctly identifying interactive biomolecules from cell lysates.[94]

4.2 DNA/RNA/PNA hybridization

Because DNA/RNA contains a large amount of negative charges in the phosphate backbones, it is ideal to use SiNW-FETs to monitor DNA/RNA hybridizations, which could cause considerable variation in the charge-carrier density on the SiNW-FET surface, leading to a significant conductance change inside the SiNW-FET.[29,58] In addition to using DNA/RNA as probe (receptor) molecules, Hahm *et al.* have used a peptide nucleic acid (PNA), an artificially synthesized polymer similar to DNA, to modify SiNW-FETs (called PNA/SiNW-FETs) for real-time DNA detections.[58] The advantage of a PNA/SiNW-FET biosensor is that PNA does not contain any phosphate groups in its backbone; thus, the binding of the PNA/DNA or PNA/RNA strands is stronger than that of the DNA/DNA or DNA/RNA duplexes due to the lower electrostatic repulsion. Moreover, PNA has a stiff chemical structure, which enables the distance of the target–receptor binding site (r_{bs}) to the SiNW surface to be well defined.[72] The chemical structure of PNA is stable over a wide pH range that makes the PNA/SiNW-FET a promising candidate for various physiological applications.

The PNA/SiNW-FET has been reported to enable the highly sensitive and rapid diagnosis of the dengue virus infection.[95] In the test, a specific fragment of the dengue virus genome sequence was amplified through a reverse-transcription-polymerase chain reaction (RT-PCR). The RT-PCR product was utilized as the target DNA to identify the existence of the dengue virus. In addition, a specific PNA with a complementary sequence of target DNA was carefully selected and modified on the SiNW-FET as the receptor. Through the hybridization between the target DNAs and receptor PNAs, an accumulation of negative charges on the SiNW surface resulting from the negatively charged DNA backbone could cause a conductance change in the SiNW-FET. Using this method, a detection limit of 10 fM for the amplicons of the dengue virus genome could be achieved, thus establishing a promising platform for virus detection.[95] PNA/SiNW-FET was also demonstrated to allow the detection of microRNA (miRNA) for early diagnosis of tumor development. The miRNAs, which involve several significant physiological pathways and various diseases, were considered to be effective biomarkers for clinical diagnosis. In addition to conventional methods, such as Northern blotting, surface plasmon resonance (SPR), and other bioluminescence-based techniques, PNA/SiNW-FET was reported to enable the label-free and direct detection of miRNA. In a study reported by Zhang *et al.*,[59] a detection limit for miRNA sensing down to 1 fM was achieved, where the PNA/SiNW-FET could not only distinguish the fully matched from one-base mismatched miRNA sequence but also detect miRNA from the total RNA extract of HeLa cells, which is always a challenge in RNA identification. A comparison of the sensitivity for miRNA sensing between the PNA/SiNW-FET and DNA/SiNW-FET was also performed. A clearly improved response was obtained with the PNA/SiNW-FET, demonstrating the advantage of using PNA as an immobilized receptor for miRNA detection.[59]

4.3 Virus detection

From influenza to AIDS, virus infection is one of the most important causes of human diseases. To prevent the outbreak of potentially hazardous virus infections, a rapid, selective, and sensitive means of detecting viruses is central to implementing an effective response to viral infection. To date, several methods have been used to confirm virus infection, including immunofluorescence assay (IFA), hemagglutination-inhibition (HI), enzyme immunoassays (EIA), and RT-PCR. Among these methods, the EIA-based techniques, which mostly target the abundant nucleoprotein in a virus, are simple and convenient but cannot distinguish among virus subtypes. RT-PCR offers the best sensitivity; however, selecting the proper primer sets becomes more challenging due to the diverse virus subtypes and the continuing evolution of a virus. Comparatively, SiNW-FETs can offer an excellent platform for monitoring a virus, which contains a considerable amount of charges to induce the conductance change in the SiNW-FET upon binding the receptor modified on the SiNW surface. For example, the H5N2 avian influenza virus (AIV) and influenza A virus were detected with SiNW-FETs modified with specific antibodies.[61,62] As demonstrated in Fig. 5, SiNW-FETs can achieve an extraordinarily sensitive and specific detection of H5N2 AIV in a very dilute concentration at the 10 attomolar (10^{-17} M) level.[62] Moreover, SiNW-FETs were also verified as being able to ultrasensitively detect the influenza A virus at a single virus level.[61]

4.4 Recording excitable cell response

Conventional techniques utilized for electrophysiological studies of excitable cells (*e.g.*, neurons, cardiomyocytes, and

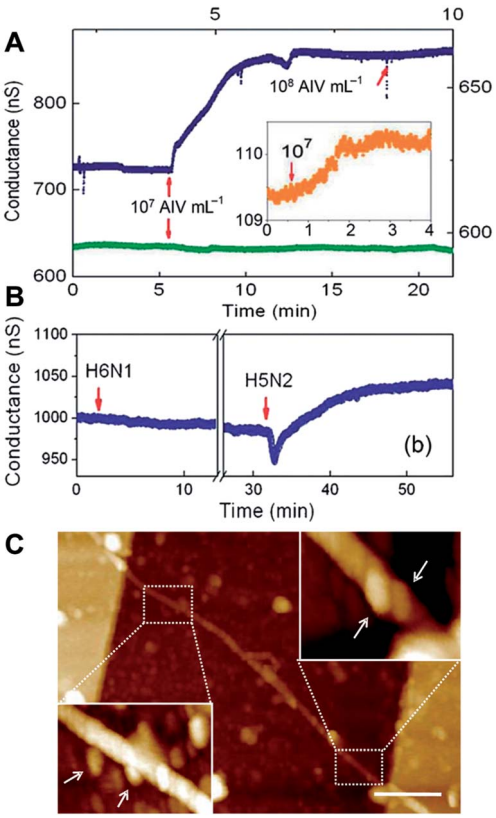

Fig. 5 The real-time detection of H5N2 AIV with a SiNW-FET modified with a monoclonal antibody against the H5N2 virus (called mAb_{H5}/SiNW-FET). (A) As depicted by the blue trace, the mAb_{H5}/SiNW-FET biosensor has a prominent electrical response to H5N2 AIV (10^7 AIV per mL). However, the biosensor only exhibits a slight variation in response to the subsequent addition of AIV (10^8 AIV per mL), most likely due to saturation of the binding sites. The arrows indicate the addition of H5N2 AIV. The green trace represents a negative control by applying a bare SiNW-FET without any surface modification for the detection of H5N2 AIV. No significant conductance change was observed after the addition of H5N2 AIV (10^7 AIV per mL). Inset: In contrast, after the bare SiNW-FET was modified with mAb_{H5} for the detection of H5N2 AIV (10^7 AIV per mL), an apparent conductance change was observed. (B) Another control test was performed using a mAb_{H5}/SiNW-FET to probe H6N1 AIV (10^8 AIV per mL). While there was no apparent electrical response to H6N1 AIV, a conductance increase was observed after the introduction of H5N2 AIV (10^7 AIV per mL), illustrating the binding specificity of the mAb_{H5}/SiNW-FET. (C) An AFM topograph of H5N2 AIVs bound on the mAbH5/SiNW-FET was taken soon after the electrical measurement of (A) was finished. The expanded scales for the bound H5N2 AIVs are displayed in the insets, where H5N2 AIV particles are marked with white arrows. The scale bar represents 1 μm. Reprinted with permission from ref. 62. Copyright Wiley-VCH Verlag GmbH & Co. KGaA.

secretory cells) with micro/nanoelectrodes have provided insight into cellular responses.[96] However, a major technical challenge remains that involves the desired recording with higher spatial resolution and large-scale multiplexing for more detailed investigations of cell physiology. NW/NT-FETs, which can afford rapid and highly sensitive electrical measurements, allow for nanoscale minimization and device integration, thus offering promising potential to realize the recording of excitable cells with high spatial resolution and large-scale mapping.[57,65,97–101]

SiNW-FETs have been recently applied as an active interface to couple with myocytes cells or heart tissues for heart rhythm recording.[97,100] The periodic beatings of cardiomyocyte cells result from the depolarization–repolarization of the membrane potential, which is induced by the transmembrane concentration gradient that is controlled by synergetic operations of various ion channels. SiNW-FETs fabricated on conventional rigid Si substrates display a high sensitivity to the local electric field established by the membrane potential and have been applied to investigate the beating rhythm in cardiomyocytes with excellent signal-to-noise ratios (typically >5).[97,99] In addition, multiplexing recording of active signals from cardiomyocyte monolayers was conducted with SiNW-FET arrays, enabling the high spatial and temporal resolution analysis for signal propagation and temporal shifts in the regime of hundreds of micrometers (~300 μm) and milliseconds. Furthermore, planar SiNW-FET arrays constructed on transparent flexible polymeric substrates were proven to offer additional advantages that cannot be realized with conventional FET devices on Si substrates. For instance, these flexible SiNW-FET arrays enable the formation of conformal coverage on samples with a 3D geometry and allow the simultaneous electrical recording and optical positioning of devices to specific regions on a sample surface.[97]

To achieve temporal and spatial resolutions down to the microsecond (μs) and a few micrometers (μm) for the investigations of subcellular biological processes, encoded ultrashort-channel SiNW-FET devices were fabricated through the alternative growth of highly and lightly doped regions along the SiNW growth direction (as illustrated in Fig. 6A).[100] Fig. 6B illustrates a short-channel NW-FET interfaced with an extracellular region of a cell. Sequentially, e-beam lithography and thermal evaporation were applied to fabricate Cr/Au pads as the source and drain electrodes. With a SiNW-FET array composed of multiple short-channel devices (indicated as d1, d2 and d3 in Fig. 6C) with various device-to-device separations, the signal propagation speeds in beating cardiomyocytes were recorded (Fig. 6D) and determined to be approximately 0.4 (between d1 and d2) and 0.8 (between d1 and d3) m s^{-1}, which are in good agreement with the reported signal transduction rate in cultured cardiomyocytes. In addition, the peak width (~500 μs) of the responses recorded with these ultrashort devices was comparable to the intrinsic time constant of the Na^+ channels and thus underlines the potential of these "pointlike" detectors in probing ion channel activity. A histogram of the time lags between devices d1 and d2 (red, separation distance 1.9 μm) and between devices d1 and d3 (blue, separation distance 73 μm) is illustrated in Fig. 6E, which demonstrates that the time lag recorded between two devices is proportional to the device separation.[100]

In addition, an elegant design of hybrid SiNW-FET arrays integrated with individual axons and dendrites enables simultaneous detection, stimulation, and/or inhibition of signal propagation in a single neuron.[65] Herein, well-oriented SiNW-FET arrays are fabricated on a substrate with patterned regions modified with poly-lysine, which was applied to guide the growth of neurons to ensure that the pre-defined SiNW-FET arrays come into contact with axons and dendrites from the same neuron. To prevent electrode corrosion in devices under the harsh conditions of cell culture and the subsequent electrical measurement, isotropic silicon nitride was deposited on the metal electrodes as a passivation layer during the device fabrication. This strategy produces a prolonged survival time of the fabricated devices for at least 10 days under cell-cultured conditions at 37 °C. After the successful construction of an integrated SiNW-neuron system with linear arrays distributed along the growth direction of the protoplasmic protrusions in the neural cells, the forward and backward propagations of the action potentials in individual axons and dendrites can be simultaneously investigated.[65]

All of these real-time, label-free and in-situ recordings of living cells demonstrate that nanoscale FET devices provide a promising tool for both fundamental and advanced investigations of the responses in excitable cells induced by both external and internal stimuli, thus facilitating advancement in future cardiology and neurology studies.

4.5 Biological kinetics

Since the pioneering work by Cui *et al.*,[19] SiNW-FETs have become a promising platform for investigations of biomolecular interactions based on the surface binding mechanism. However, most of the studies using SiNW-FETs have been focused on reducing the detection limit, with relatively little effort expended on quantifying the binding–unbinding kinetics of the target–receptor interactions. In addition to recent achievements in femtomolar sensing in immunodetection,[21,60] several mathematical models have been developed to rationalize the quantitative interpretation of binding kinetics determined by SiNW-FET biosensors.[102,103]

For the real-time sensing of DNA hybridization, ssDNA was immobilized on SiNW-FETs as a receptor to detect the presence of complementary DNA strains. To determine the kinetics of a surface binding assay (*i.e.*, DNA hybridization) conducted in flowing microfluidic systems, a mathematical model was developed.[104] In this model, at high analyte flow speeds (>0.5 mm s^{-1}), an ordinary differential equation derived from the Langmüir binding model was applied to describe the binding event:

$$\frac{d\Theta_t}{dt} = k_{on}C(\Theta_{max} - \Theta_t) - k_{off}\Theta_t, \quad (4)$$

where Θ_t is the surface density of the bound analytes; k_{on} and k_{off} represent the rate constants of association and dissociation,

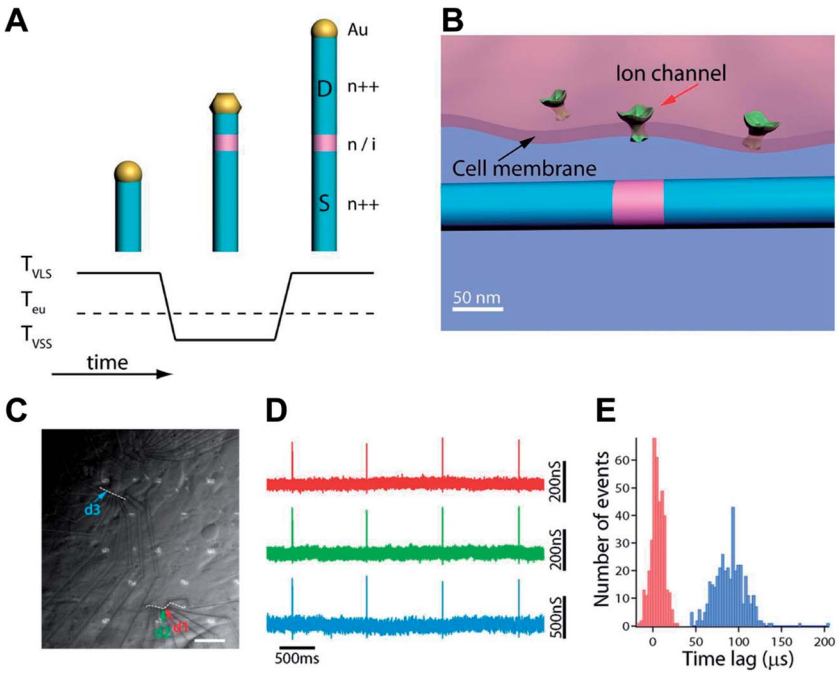

Fig. 6 (A) An illustration of the gold-nanocluster-catalyzed growth of a NW, which displays a well-controlled axial dopant profile introduced during vapor-solid-solid (VSS) growth. Initially, an n^{++} source (S) electrode is synthesized *via* the vapor-liquid-solid (VLS) mechanism. Subsequently, either n or i active device regions are encoded by VSS growth. Lastly, another VLS phase of growth completes the n^{++} drain (D) electrode. (B) A schematic of a short-channel NW-FET interfaced with an extracellular region of a cell. (C) An optical image of cardiomyocytes interfaced with three devices (labeled d1, d2, and d3) with a 130 nm channel length. The white dashed lines represent the NW positions. The scale bar is 15 μm. (D) Representative recorded signals from d1 (red), d2 (green), and d3 (cyan). (E) A histogram of the time lags between devices d1 and d2 (red, separation distance 1.9 μm) and between devices d1 and d3 (blue, separation distance 73 μm). Reprinted with permission from ref. 100. Copyright the American Chemical Society.

respectively; C is the concentration of the analytes; and Θ_{max} refers to the maximum number of binding sites available per surface area. The analytical solution of eqn (4) can be solved as:

$$\Theta_t = \frac{k_{on} C \Theta_{max}}{k_{on} C + k_{off}} \left(1 - e^{-\left(k_{on} C + k_{off}\right) t}\right). \quad (5)$$

To correlate the measured resistance changes (ΔR) in the SiNW-FET caused by the analyte-receptor binding with the surface density (Θ_t) of the bound analytes (*i.e.*, target ssDNA), eqn (6) was developed:

$$\Theta_t = \frac{k_{on} C \Theta_{max}}{k_{on} C + k_{off}} \left(1 - e^{-\Delta R/(R_{max} - R_t)}\right), \quad (6)$$

where $\Delta R = R_t - R_0$; R_t is the resistance measurement with the SiNW-FET at time t; R_0 is the resistance measurement at $t = 0$; and R_{max} represents the resistance measured at the saturation of the bound analytes. Eqn (6) was considered to be a rational relationship between ΔR and Θ_t according to experimental observations that Θ_t is an exponential function of $\Delta R/R_0$ at saturation and two imposed boundary conditions: (1) the measured resistance reaches its saturation level when the maximum number of binding events occurs following the Langmüir binding model, and (2) the measured resistance is unchanged from its starting level when a zero binding event is involved.[102] Based on these assumptions, it was estimated that the surface density of the bound analyte molecules is related to the resistance change (eqn (5) and (6)) as

$$\Theta_t = \frac{k_{on} C \Theta_{max}}{k_{on} C + k_{off}} \left(1 - e^{-\left(k_{on} C + k_{off}\right) t}\right) = \frac{k_{on} C \Theta_{max}}{k_{on} C + k_{off}} \left(1 - e^{-\Delta R/(R_{max} - R_t)}\right). \quad (7)$$

The fractional occupancy of the binding sites (*i.e.*, the immobilized ssDNA receptors) can be further described as

$$\frac{\Theta_t}{\frac{k_{on} C}{k_{on} C + k_{off}} \Theta_{max}} \text{ (fractional occupancy)} = 1 - e^{-\left(k_{on} C + k_{off}\right) t} = 1 - e^{-\Delta R/(R_{max} - R_t)}. \quad (8)$$

The relationship between the kinetic constants and resistance measurements, as described in eqn (8), was verified by the agreement between the time-dependent fractional saturation curve determined with SPR-derived kinetic parameters (k_{on} and k_{off}) and that with the SiNW-FET sensing measurements (R and ΔR). This proposed model then provides an intuitive description to correlate binding parameters and resistance measurements:

$$(k_{on} C + k_{off}) t = \Delta R/(R_{max} - R_t). \quad (9)$$

Consequently, the DNA hybridization kinetics can be quantitatively assessed with the experimentally measured electrical response with SiNW-FET sensors.

In addition, to reduce the discrepancy in the quantitative analysis resulting from the device-to-device variation among the SiNW-FET sensors, a normalization of the absolute electrical response (ΔI_{sd}) with the sensor gate dependence ($g_m = dI_{sd}/dV_g$, the transconductance of the SiNW-FET device) was applied.[77,105] A combination of the normalized response ($\Delta I_{sd}/g_m$) with the Langmüir isotherm yields analytical models that enable the effective determination of the binding affinities and kinetics of typical target–receptor complexes. In a fast mixing condition with no mass transportation limitation, the absorption and desorption of binding pairs can be described with eqn (10) and (11), respectively:[103]

$$\frac{I_{sd}(t)}{g_m} = V_{eq}\left(1 - e^{-\left(k_{on}[c]+k_{off}\right)t}\right) \quad (10)$$

$$\frac{I_{sd}(t)}{g_m} = V_{eq}e^{-k_{off}t} + V_r, \quad (11)$$

where $I_{sd}(t)$ represents the source–drain current measurement at time t; V_{eq} is related to the analyte charge and concentration, capacitive coupling, surface density of the binding sites, and association constant of the target–receptor binding;[104] C is the concentration of the analytes; and V_r represents the sensor response induced by a small portion of bound molecule residues after analyte desorption.

Using eqn (10) and (11), the kinetic parameters for both the association and dissociation phases of binding can be obtained by fitting the experimental responses in the $I_{sd}(t)/g_m$ *vs.* C and $I_{sd}(t)/g_m$ *vs.* t measurements with the SiNW-FETs. In addition, because of the use of the normalized sensor response, which greatly reduces the signal fluctuation induced by device-to-device variations, a more quantitative analysis of the sensor response in the SiNW-FET arrays can be achieved, thus greatly facilitating the advancement of high-throughput multi-channel SiNW-FET sensors.

4.6 Clinical diagnosis

In clinical diagnosis, biomarkers are considered to be reliable molecular signatures for identifying disease occurrence, pathology states, and responses to medical therapy. However, during the early stage of disease pathogenesis, the detection of biomarkers is critically challenging due to the extremely low concentration of these signature species and possible interference from complicated compositions in physiological samples. NW-FET biosensors, which can provide highly sensitive, label-free and real-time detection, are thus considered promising for detecting biomarkers.[60,106]

Recently, several successful applications of SiNW-FETs in disease identification have been demonstrated. For example, cardiac troponin I has been suggested as a highly sensitive and specific biomarker to detect acute myocardial infarction.[107] The antibodies of cardiac troponin I were immobilized on a SiNW-FET in tests, where a detection limit of 0.092 ng L^{-1} with a wide linear dynamic range of 0.0092–46 ng mL^{-1} for cardiac troponin I examination was achieved.[108] To improve the accuracy of a screening test for clinical diagnosis, simultaneous detection of multiple biomolecular species is considered to be more beneficial than examinations that rely on only a single biomarker. SiNW-FET devices, which are feasible to use in the construction of an array configuration, have been fabricated for the multiplexed detection of cancer markers. As a representative example,[60] antibodies of three different cancer markers (prostate specific antigen, carcinoembryonic antigen, and mucin-1) were immobilized individually on three different SiNW-FET devices in a sensorial array. The high detection selectivity of each SiNW-FET device was demonstrated to enable the simultaneous recording of each cancer marker independently with a detection limit down to 0.9 pg mL^{-1} in undiluted serum samples.[60]

For studies of biomarkers in whole blood samples, the limited Debye–Hückel length (λ_D) resulting from a high salt concentration in physiological fluids induces a significant screening effect on the electrical measurements by a SiNW-FET. To solve this problem, pre-purification of the target analytes and an exchange of the high salt buffer with a low salt electrolyte are required. An integrated system that combines a microfluidic purification chip (MPC) with a label-free SiNW-FET sensor has been reported to overcome the difficulties encountered in whole blood samples.[109] With this MPC-FET system, target biomarkers in blood samples, the prostate specific antigen and carbohydrate antigen 15.3, were first captured by primary antibodies of each antigen. A washing step followed in the MPC system to exchange the blood fluid with the sensing buffer with low ionic strength. Induced by exposure of the MPC system to UV irradiation, a cleavage of antigen–antibody complexes occurred, and the released antigen–antibody complexes were then eluted to the sensing system for the final detection of the target biomarkers with multiple SiNW-FET devices.[109]

5 Innovative SiNW-FET architecture

5.1 3D FET nano-probe

SiNW-FETs have been utilized to record extracellular electrical signals;[57,65,97–99,110] however, these FET devices are placed on planar substrates, making it difficult to locally probe the signals from individual cells. The development of a movable 3D nanoscale FET that can be moved to be in contact with or even injected into a cell is worthwhile. Tian *et al.*[68] and Xu *et al.*[111] have successfully fabricated movable 3D nano-FETs through the synthetic integration of kinked SiNWs.[112] These kinked SiNWs represent a new class of NW building blocks that can be used to construct the functional devices of 3D nano-FETs with geometrically controlled NW superstructures. The kinked SiNW-FET superstructures can be well controlled during the synthesis of SiNWs in a CVD reaction *via* the VLS mechanism by varying the reactant pressure and the concentrations of the reacting gases. As illustrated in Fig. 7A and B,[68] ultra-short SiNW-FET devices with the nano-FET sensing element (pink color in Fig. 7A, lightly doped SiNW) and the source and drain electrodes (blue color in Fig. 7A, heavily doped SiNW) were synthesized by delicately controlling the dopant (phosphorus) concentrations during the SiNW growth *via* a CVD reaction.

Fig. 7C presents an image of a fabricated 3D nano-FET probe, where the FET is located at the tip of an acute-angle kinked SiNW connected with nanostructure arms composed of multilayer photoresists.

This 3D nano-FET probe has been successfully inserted into a single living cell to measure the intracellular electrical signal, as illustrated schematically in Fig. 7D.[68] In this application, phospholipid bilayers were first coated on the nano-FET surface to facilitate the insertion of the nano-FET into the cell through the fusion of the coated phospholipid bilayers with the cell membrane. The strategy of coating the probe surface with lipid bilayers is critical in the assistance of a rigid probe to access the inner cellular region for intracellular electrical recording.[112,113] Fig. 7E presents optical images of the process of a phospholipid-modified 3D nano-FET approaching an HL-1 cell; correspondingly, a diagram of the measured potential changes when the 3D nano-FET comes in contact with an isolated HL-1 cell is presented in Fig. 7F. The potential recorded displayed a sharp drop (~50 mV within 250 ms) when the probe moved across the interface of the cell membrane (region I of Fig. 7F), remained almost constant when the probe tip stayed within the cell interior (region II of Fig. 7F), and then returned to the baseline when the probe was removed from the intracellular space of the target cell (region III of Fig. 7F). These experimental results demonstrate that functional kinked SiNWs synthesized using bottom-up techniques can be configured to a 3D nano-probe for applications in life sciences, including intracellular and deep tissue/cell recordings, which are difficult to achieve using present top-down methods.[63]

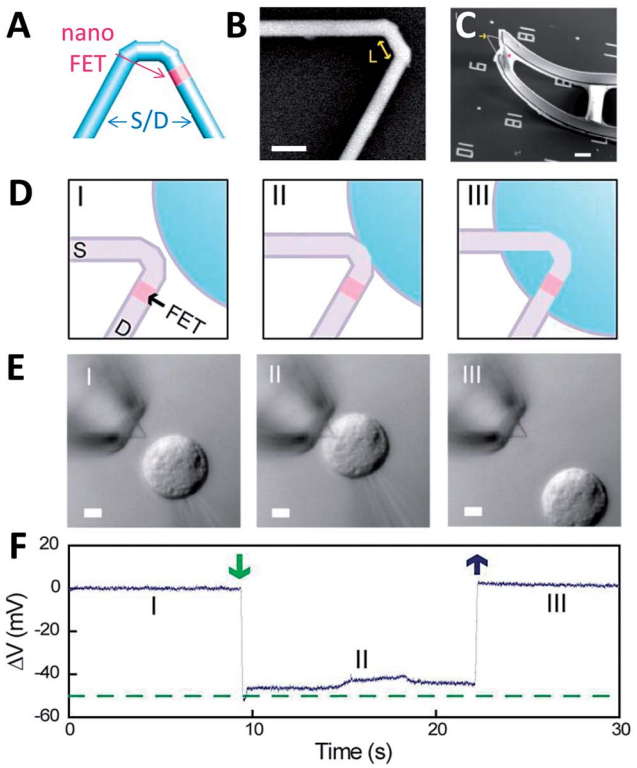

Fig. 7 (A) An illustration of the 60° *cis* multiple kinked configuration in the SiNW structure. The blue and pink regions designate the source–drain (S–D) and nanoscale FET channel (80 nm in diameter and ~20 nm in length), respectively. (B) An SEM image of a doubly kinked SiNW with a *cis* configuration. *L* is the length of the segment between two adjacent kinks. (C) An SEM image of an as-prepared 3D kinked SiNW probe. The yellow arrow and pink star represent the nanoscale FET and SU-8 photoresist, respectively. (D) Schematic diagrams of a SiNW probe entering a cell. The dark purple, light purple, pink, and blue colors denote the phospholipid bilayers, heavily doped NW segments, active sensor segment, and cytosol, respectively. (E) Differential interference contrast (DIC) microscopic images and (F) electrical recording from an HL-1 cell with the 60° kinked SiNW probe as the cell (I) approaches, (II) contacts and internalizes, and (III) retracts from the cellular interior. A pulled-glass micropipette (inner tip diameter ~5 μm) was used to manipulate and voltage clamp the HL-1 cell. The dashed green line represents the micropipette potential. All of the scale bars are 5 μm except that of (B) is 200 nm. Reprinted with permission from ref. 68. Copyright American Association for the Advancement of Science.

5.2 Branched nanotube-FET

To enable intracellular measurement with improved spatial resolution and reduced invasiveness of the cellular membrane, an innovative structure of SiNW-FET devices called a branched intracellular nanotube-FET (BIT-FET) has been developed.[114] Compared with a conventional SiNW-FET, the BIT-FET was constructed with an additional taped hollow nanotube standing up on the SiNW and oriented approximately perpendicularly to the substrate surface, as illustrated in Fig. 8A. After modifying the branched nanotube with a phospholipid, which again facilitates the internalization of the nanotube into a cell through lipid fusion, the nanotube is allowed to spontaneously penetrate the cellular membrane through gentle contact with the cell without applying an external force. Because of the spontaneous penetration of the nanometer-sized probe, a tight seal between the invasive nanotube and cell membrane is formed (Fig. 8B). With this BIT-FET device, the cellular interior can come into contact with the SiNW sensing region located at the root of the hollow SiO_2 nanotube. When changes in the transmembrane potential (V_m, the difference in the electrical potential between the exterior and interior of the cell) occur that involve variations in the electrical potential of the cellular interior, corresponding changes in the conductance of the FET can be recorded. For cardiomyocytes, typical values of the resting membrane potential are approximately −90 mV, meaning that the cellular interior has a more negative voltage compared with the cellular exterior. However, during the action potential, a positive shift in V_m occurs and reaches a value of about +20 mV; in other words, the cellular interior now has a more positive potential *versus* the cellular exterior. When a p-type BIT-FET was utilized for intracellular recording, a positive shift in V_m resulted in a negative shift in the recorded conductance. Consequently, an inverted relationship was observed between the polarity of the change in conductance (G) and that in V_m (Fig. 8C).

Stable electrical recordings at a given cellular position from multiple penetration/retraction manipulations over an hour were performed using this BIT-FET system. Based on the recorded signals, no obvious degradation in either the cellular viability or recorded signals was observed, demonstrating the

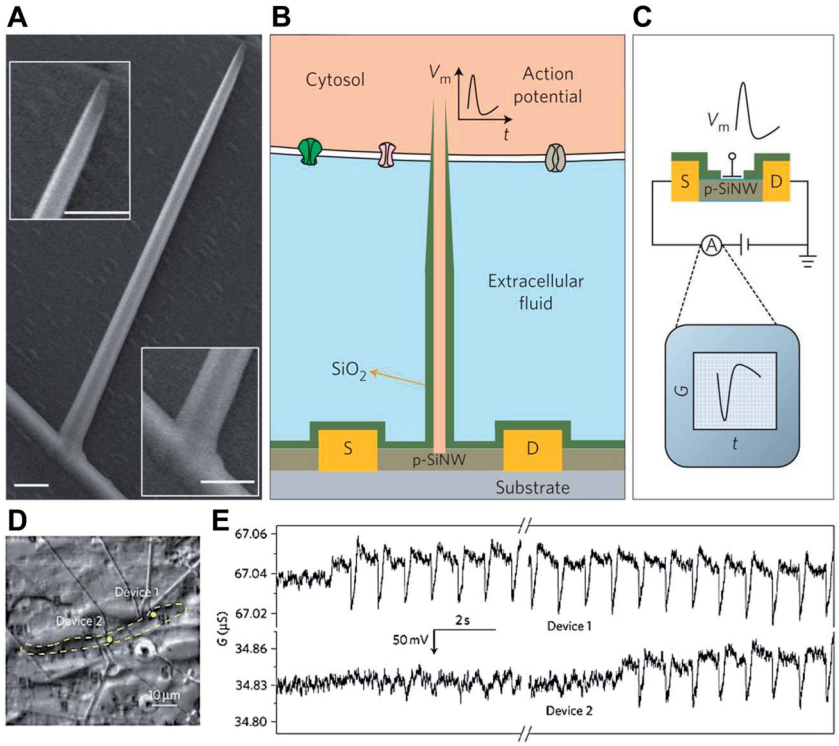

Fig. 8 (A) An SEM image of a nanotube on a SiNW. Insets: magnified images of the top and bottom of the nanotube. The scale bars are 200 nm. (B) A schematic diagram showing a cell coupled to a BIT-FET device and (C) the variation in the device conductance (G) with time t during an action potential V_m. S and D represent the source and drain electrodes. The SiO_2 nanotube connects the cytosol (orange) to the p-type SiNW-FET and, together with the SiO_2 passivation (green), excludes the extracellular medium (light blue) from the active device channel. The structures on the membrane represent different ion channels and are not scaled to the true size of the BIT-FET. (D) A DIC microscopy image of two BIT-FET devices (positions marked with dots) coupled to a single cardiomyocyte cell. The cell boundary is marked by the yellow dashed line. (E) Simultaneously recorded traces from the two devices in (D) are illustrated. The transition from the extracellular to intracellular recording can be observed in both traces but occurs in a sequential manner. The break mark labels the ~1 s discontinuity between the two adjacent traces. Reprinted with permission from ref. 114. Copyright Nature Publishing Group.

robustness and reusability of the BIT-FET device.[114] In addition, it is feasible to integrate the BIT-FET design with an array-like construction for multiplexed sensing. For this application, two aligned phospholipid-modified BIT-FETs with a separation of ~20 μm were interfaced with a single cardiomyocyte cell, as illustrated in Fig 8D. The recorded signals from both BIT-FETs exhibit an upward shift in the baseline conductance followed by a series of spike-like recordings (Fig 8E). The changes in the baseline conductance are correlated with the initial penetration of the cell membrane with the nanotube of the BIT-FET, and a time lag of ~10 seconds was observed between these two BIT-FET devices. In addition, the recorded spike-like signals indicate changes in the intracellular action potential and display a frequency that is consistent with the beating rate of the cardiomyocyte under study. Based on these preliminary studies, the advanced construction of integrating the BIT-FET design with conventional large arrays of FETs is promising for high-throughput multiplexed measurements with high spatial and temporal resolutions.

5.3 Sub-nano structure FETs

SiNW-FETs produced using top-down techniques are clearly advantageous because of the exact wire size located in a precise position at the wafer-scale. However, it is difficult to reduce the size of a SiNW down to sub-20 nm with top-down approaches due to the resolution limit of the lithography process; consequently, this size limitation might impede a SiNW having a high surface-to-volume ratio. Thus, Seol *et al.*[115] reported on selectively modified SiNWs with a nano-forest structure that is self-aligned in a top-down fabricated SiNW. The formation of the nano-forest was achieved by selective exposure of the channel region of a SiNW-FET followed by metal-assisted chemical etching. Benefiting from the notable characteristics of metal-assisted chemical etching, which include constant etching directionality, etching uniformity, and the generation of a nanoscale profile, a bundle of vertically standing Si nanostructures, named a nano-forest, was formed on the surface of a SiNW. The height of the forest structure increased with a longer etching time. This nano-forest morphology thus significantly enlarges the surface-to-volume ratio of a SiNW, resulting in a greater sensitivity.[115] As illustrated in Fig. 9, the SiNW-FET with the sub nano-forest structure displays an enhanced conductance modulation for a porphyrin–Si hybrid device. Porphyrin, which is a photoactive organic material in chlorophyll, is utilized in this hybrid system to provide a reliable photoinduced charge transfer (PCT) process. The PCT efficiency between the

porphyrin and the SiNW, caused by external optical excitation, is clearly increased with the nano-forest-modified SiNW compared with the initial SiNW. This study demonstrates that tailoring the morphology of materials in the nanometer regime is vital to improve the performance and sensitivity of SiNW-FETs and other types of nanoscale devices.

5.4 Lipid-bilayer-modified FETs

Every single cell in a living organism is confined by a membrane structure that helps to maintain the structural integrity of the cell and plays an active role in the transport of cellular materials into and out of the cell. The structure of the membrane is mainly exemplified by lipid bilayers, in which various functional proteins responsible for various cellular activities are embedded. Synthetic phospholipid bilayers replicate the nature of cellular membranes and can afford a natural environment to support and organize membrane proteins and receptors. The integration of biomaterials and nanoelectronics provides a great opportunity to unveil the mechanisms behind intricate biological processes. Taking advantages of the excellent sensitivity and selectivity that are conferred by conventional FET devices, many research groups demonstrated the possibility of integrating lipid bilayers on NWs, NTs, and graphene to study the signal transduction pathways of membrane proteins, ion channels, pumps, motors and other carriers.[101,116–118] Recently, the signaling mechanisms of voltage-gated and ligand-gated channels have been successfully demonstrated by incorporating these channel proteins into the artificial lipid bilayers mounted on SiNW-FETs.[116,118] As demonstrated in Fig. 10, the transportation of a proton through the peptide channels embedded on the lipid bilayer modified on a SiNW-FET was investigated under various gate voltages. When the lipid bilayer on the SiNW contained gramicidin A ion-channels, changes in the solution pH could be detected. In contrast, when the membrane channels were blocked by divalent cations, the device responses were significantly suppressed. Moreover, when a voltage-gated channel, alamethicin (ALM), was embedded into the lipid bilayer (Fig. 10A), the gate voltages applied to the FET device could be utilized to modulate the opening/closing of the ion channels. Under a positive gate voltage (V_g = 0.15 V, Fig. 10B), the ALM pores opened to allow the inflow of protons. Thus, changes in the solution pH can be investigated based on the variation in the electrical signals recorded with the SiNW-FET device. In contrast, when the gate voltage was set back to 0 V (Fig. 10C), the ALM pores closed, and the pH sensitivity of the device diminished.[101] These studies demonstrate the significance of lipid-bilayer-modified FET devices acting as excellent biosensors to facilitate investigations of fundamental functions of various biomolecules, such as the ion channel proteins under study.

6 Future challenges

Based on their ultra-sensitive, highly selective, label-free and real-time molecular recognition capabilities, NW-FETs can be used as promising biosensors employed for biological analysis and cellular investigation. Despite these merits, technical challenges and environmental confrontations remain before NW-FETs can serve as practical instruments in biosensing measurements.

6.1 Neutral molecule detection

FET-based biosensors are typically useful in the detection of charged species, such as DNA, RNA, proteins, viruses, *etc.* These charged species with their self-established electric field, when approaching or captured on the sensor surface, are beneficial for modulating the electrical conductivity inside an FET biosensor. In contrast, neutral molecules, or biomolecules that bear only a slight charge density, are detrimental to detections by FET-based biosensors. Thus, special methodologies are required for the detection of neutral targets. As one of the possible resolutions, the binding site of a receptor for the neutral target can be designed to be preoccupied by a charged reporter molecule (CRM) before the

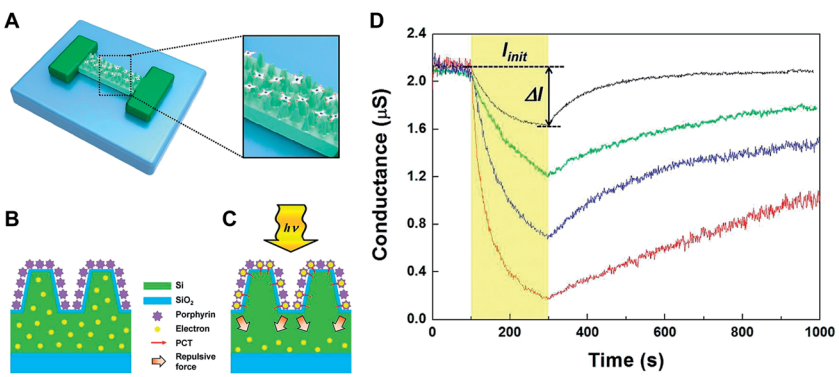

Fig. 9 (A) A schematic diagram of the porphyrin–SiNW hybrid device. (B) An illustration that shows the electron distribution of the modified SiNW in a dark environment. (C) An illustration that shows the photoinduced charge transfer (PCT) behavior and resulting electron distribution of the modified SiNW during light illumination. (D) Transient characteristics of recorded conductance measurements with modified SiNWs. The black (top), green, blue, and red (bottom) curves are recorded from the unetched SiNW, 10 s etched SiNW, 20 s etched SiNW, and 30 s etched SiNW, respectively. The voltages applied for the devices were 1.0, 1.05, 1.12 and 1.22 V, respectively. Reprinted with permission from ref. 115. Copyright the American Chemical Society.

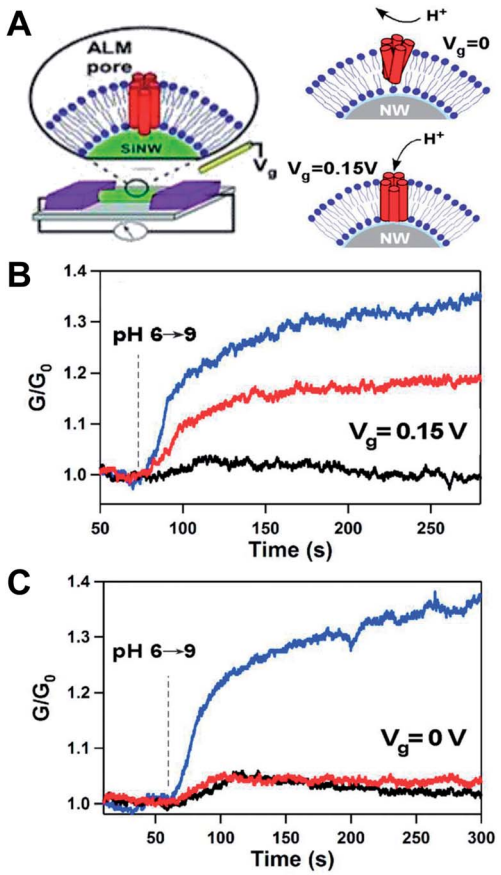

Fig. 10 Voltage-gated operation of the SiNW-FET device incorporated with alamethicin (ALM) pores. (A) A schematic diagram illustrates the mechanism of voltage-gated proton transport through self-assembled ALM pores in the lipid bilayer coated on a SiNW-FET. (B) Time traces of normalized conductance recorded as the pH of the solution was changed from 6 to 9 for the uncoated SiNW-FET (blue trace), lipid-bilayer-coated SiNW-FET (black trace), and lipid-bilayer-coated SiNW-FET incorporating ALM pores (red trace). The gate bias was held at V_g = 0.15 V. (C) Time traces of a similar experiment recorded at V_g = 0 V. The vertical dashed lines indicate the time when the pH of the injected flow in the fluid cell was switched from 6 to 9. Reprinted with permission from ref. 101. Copyright National Academy of Science, USA.

neutral target binds. To prevent the CRM from escaping from the FET sensor, this CRM is delicately designed to be chained, with a chemical linker, in the proximity of the SiNW surface. Upon the binding of the neutral target, the preoccupied CRM is expelled out of the binding site, moving nearby the FET surface and exerting an electric field to modulate the sensorial conductance. As an example, a SiNW-FET modified with a specifically designed receptor, a steroid-binding protein chained with a CRM, was demonstrated to be able to detect uncharged steroid.[119,120] When the binding of steroid occurred, this negatively CRM, which initially occupied the steroid-binding site, was expelled from the binding site and approached the SiNW surface. Consequently, an electric signal in the SiNW-FET, induced by the expelled CRM, was observed as a result of the detection of the neutral steroid.

Other sensing techniques that induce a conductance change in the FET-based sensor without directly resorting to the charge (*i.e.*, electric field) are also suitable for neutral molecule detection. For instance, the frequency-domain detection of biomolecules using a SiNW-FET by Zheng *et al.* (as discussed in Section 3.4.2)[80] may be considered as another option for neutral molecule detection. The cause of the 1/*f* noise in the power spectral scan is associated not only with the target–receptor binding–unbinding rates but also with the variation of both the resistance and capacitance coupling to the FET sensing system during a sensing measurement. The target–receptor binding, including the case of the binding of neutral target molecules, can be analyzed from the characteristic frequency of the Lorentzian spectral shape in the 1/*f* spectrum.

Despite these feasible tactics for neutral molecule detection using a SiNW-FET, innovative methodologies for the sensitive, effective, and practical detection of significant neutral biological species are in high demand in the contemporary development of FET-based biosensors.

6.2 Sensing in a high salt buffer

Detecting target analytes in a high salt buffer is cumbersome for FET-based measurements but is frequently encountered for an FET biosensor applied in biological experiments. As discussed earlier, the sensing mechanism of an FET-based biosensor relies on conductance modulation by the interacting electric field exerted from the bound molecular charges. However, the interacting electric field suffers from the Debye–Hückel screening effect in physiological buffer solution (*e.g.*, 1× PBS, a high salt buffer of strong ionic strength with λ_D = 0.7 nm), which accordingly reduces the electrical signals during observation. Therefore, determining how to perform an effective electrical measurement in a high salt buffer is critical for advancing FET-based devices in the biosensing modality.

Although a two-stage method was successfully implemented for the label-free detection of biomarkers by a SiNW-FET from the complex environment of whole blood (or any other physiological fluid), as discussed in Section 4.6,[109] this approach involves sample purification in the first step and target detection in the second stage. First, a microfluidic purification chip simultaneously captures multiple biomarkers from blood samples. In the second step, the captured biomarker–receptor complexes are released under photoinduced cleavage and, after washing, are mixed with the purified buffer (of weak ionic strength with a long λ_D) and finally guided into a reservoir for sensing by a SiNW-FET.

While this exquisite design of purification and detection in two separated steps works well for the effectual sensing of target analytes in a high salt buffer, other practical detections with FET-based biosensors capable of performing sufficient analysis for clinical diagnosis, which is conducted mostly in a high salt buffer, are needed.

6.3 High-throughput multiplexed sensing

For adequate disease treatment, ensuring accurate diagnosis and monitoring the response to applied medical

implementation are both critical. Thus, a multiple-biomarkers test is regarded as being more efficient for the diagnosis of complex diseases (*e.g.*, cancer), where the disease heterogeneity likely makes a diagnosis that relies on a single-biomarker test questionable. Zheng *et al.* utilized three SiNW-FET arrays modified with distinct receptors for multiplexed sensing and demonstrated the simultaneous electrical detection of three cancer markers.[60] Although the SiNW-FET arrays have the potential to enable multiplexed sensing, more sophisticated designs for both device fabrication and signal acquisition are highly desirable for future advancements to achieve high-throughput detections with higher device performance and sensing efficiency.

7 Summary

Traditional biosensors usually require a significant amount of the sample for tests due to their relatively low detection sensitivity; in contrast, nanoscale-material-configured biosensors can be fabricated to possess high detection sensitivity to minimize the sample consumption. In this review, we have first described the working principles and device properties of SiNW-FETs. To perform as a reusable, calibratable biosensor for quantitative analysis, the surface of a SiNW-FET can be modified with reversible association–dissociation pairs, such as GSH/GST-tag[24] and Ni^{2+}/His_6-tag,[74] or cleavable disulfide bonds.[62] Several methods to improve the detection sensitivity of a SiNW-FET biosensor are also introduced.

SiNW-FET biosensors have been successfully applied in biological and cellular studies, including protein–protein interaction, DNA/RNA/PNA hybridization, virus detection, excitable cell response recording, biological kinetics, and clinical diagnosis. In particular, the feasibility of detecting target analytes from a cocktail solution, such as blood,[109] makes SiNW-FETs a promising tool for future medical applications. Moreover, SiNW-FETs are able to integrate with live cells, *e.g.*, neurons, demonstrating that this nanoscale gadget can be implanted in living biological systems for advanced clinical investigations.[97] We also exemplified the successful constructions of 3D FET nano-probes, branched nanotube-FETs, sub-nano structure FETs and lipid-bilayer-modified FETs as representative examples of the recent developments of innovative SiNW-FET architectures.

While SiNW-FETs have exhibited many performance merits in various biosensing applications, challenges remain for future advancements in FET-based biosensors. In this review, we noted some typical challenges, such as the detection of significant neutral biological molecules with FET devices, sensing the whole blood sample within serum of high ionic strength that requires a desalting step before the analysis by FET, the demand for new designs of novel device fabrication and signal acquisition systems for high-throughput multiplexed sensing, and the mass production of robust nanoscale FET devices to realize practical applications in point-of-care diagnosis. Notwithstanding these challenges, we believe that nanoscale FET-based biosensors have played and will continue to play a significant role in biological analysis and cellular investigation in the future.

Abbreviations

AAM	All area modification
CaM	Calmodulin
CNT	Carbon nanotube
CRM	Charged reporter molecule
CVD	Chemical vapor deposition
DIC	Differential interference contrast
DNA	Deoxyribonucleic acid
EDTA	Ethylenediaminetetraacetic acid
FET	Field-effect transistor
GSH	Glutathione
GST	Glutathione *S*-transferase
His_6-tag	Hexahistidine-tag
miRNA	MicroRNA
MPC	Microfluidic purification chip
PBS	Phosphate buffered saline
PCT	Photoinduced charge transfer
PNA	Peptide nucleic acid
RNA	Ribonucleic acid
RT-PCR	Reverse transcription-polymerase chain reaction
SiNW	Silicon nanowire
SiNW-FET	Silicon nanowire field-effect transistor
SOI	Silicon on insulator
ssDNA	Single-stranded DNA
SSM	Selective surface modification.

References

1 D. R. Thevenot, K. Toth, R. A. Durst and G. S. Wilson, *Biosens. Bioelectron.*, 2001, **16**, 121.
2 D. Grieshaber, R. MacKenzie, J. Voros and E. Reimhult, *Sensors*, 2008, **8**, 1400.
3 S. Viswanathan, H. Radecka and J. Radecki, *Monatsh. Chem.*, 2009, **140**, 891.
4 M. Farre and D. Barcelo, *TrAC, Trends Anal. Chem.*, 2003, **22**, 299.
5 Y. Wang, H. Xu, J. M. Zhang and G. Li, *Sensors*, 2008, **8**, 2043.
6 S. Rodriguez-Mozaz, M. J. L. de Alda and D. Barcelo, *Anal. Bioanal. Chem.*, 2006, **386**, 1025.
7 A. J. Qavi, A. L. Washburn, J.-Y. Byeon and R. C. Bailey, *Anal. Bioanal. Chem.*, 2009, **394**, 121.
8 F. M. Raymo and I. Yildiz, *Phys. Chem. Chem. Phys.*, 2007, **9**, 2036.
9 N. C. Tansil and Z. Q. Gao, *Nano Today*, 2006, **1**, 28.
10 A. M. Morales and C. M. Lieber, *Science*, 1998, **279**, 208.
11 J. T. Hu, T. W. Odom and C. M. Lieber, *Acc. Chem. Res.*, 1999, **32**, 435.
12 X. F. Duan, Y. Huang, Y. Cui, J. F. Wang and C. M. Lieber, *Nature*, 2001, **409**, 66.
13 N. L. Rosi and C. A. Mirkin, *Chem. Rev.*, 2005, **105**, 1547.
14 X. G. Liang and S. Y. Chou, *Nano Lett.*, 2008, **8**, 1472.
15 I. Willner and E. Katz, *Bioelectronics: From Theory to Applications*, Wiley-VCH, 2005.

16 M. J. Madou, *Fundamentals of Microfabrication and Nanotechnology (Volume I): Solid-State Physics, Fluidics, and Analytical Techniques in Micro- and Nanotechnology*, CRC Press, 2012.
17 M. J. Madou, *Fundamentals of Microfabrication and Nanotechnology (Volume II): Manufacturing Techniques for Microfabrication and Nanotechnology*, CRC Press, 2012.
18 M. J. Madou, *Fundamentals of Microfabrication and Nanotechnology (Volume III): From MEMS to Bio-MEMS and Bio-NEMS: Manufacturing Techniques and Applications*, CRC Press, 2012.
19 Y. Cui, Q. Q. Wei, H. K. Park and C. M. Lieber, *Science*, 2001, **293**, 1289.
20 S. J. Tans, A. R. M. Verschueren and C. Dekker, *Nature*, 1998, **393**, 49.
21 E. Stern, J. F. Klemic, D. A. Routenberg, P. N. Wyrembak, D. B. Turner-Evans, A. D. Hamilton, D. A. LaVan, T. M. Fahmy and M. A. Reed, *Nature*, 2007, **445**, 519.
22 K.-I. Chen, B.-R. Li and Y.-T. Chen, *Nano Today*, 2011, **6**, 131.
23 Y. X. Liu, X. C. Dong and P. Chen, *Chem. Soc. Rev.*, 2012, **41**, 2283.
24 T.-W. Lin, P.-J. Hsieh, C.-L. Lin, Y.-Y. Fang, J.-X. Yang, C.-C. Tsai, P.-L. Chiang, C.-Y. Pan and Y.-T. Chen, *Proc. Natl. Acad. Sci. U. S. A.*, 2010, **107**, 1047.
25 W. R. Yang, K. R. Ratinac, S. P. Ringer, P. Thordarson, J. J. Gooding and F. Braet, *Angew. Chem., Int. Ed.*, 2010, **49**, 2114.
26 Y. Ohno, K. Maehashi, Y. Yamashiro and K. Matsumoto, *Nano Lett.*, 2009, **9**, 3318.
27 T. Cohen-Karni, Q. Qing, Q. Li, Y. Fang and C. M. Lieber, *Nano Lett.*, 2010, **10**, 1098.
28 C. Li, M. Curreli, H. Lin, B. Lei, F. N. Ishikawa, R. Datar, R. J. Cote, M. E. Thompson and C. W. Zhou, *J. Am. Chem. Soc.*, 2005, **127**, 12484.
29 A. Choi, K. Kim, H. I. Jung and S. Y. Lee, *Sens. Actuators, B*, 2010, **148**, 577.
30 S. Liu and X. Guo, *NPG Asia Mater.*, 2012, **4**, e23.
31 G. Gruner, *Anal. Bioanal. Chem.*, 2006, **384**, 322.
32 S. Roy and Z. Gao, *Nano Today*, 2009, **4**, 318.
33 M. Zheng, A. Jagota, E. D. Semke, B. A. Diner, R. S. McLean, S. R. Lustig, R. E. Richardson and N. G. Tassi, *Nat. Mater.*, 2003, **2**, 338.
34 A. Star, E. Tu, J. Niemann, J.-C. P. Gabriel, C. S. Joiner and C. Valcke, *Proc. Natl. Acad. Sci. U. S. A.*, 2006, **103**, 921.
35 K. Maehashi, T. Katsura, K. Kerman, Y. Takamura, K. Matsumoto and E. Tamiya, *Anal. Chem.*, 2007, **79**, 782.
36 M. Lee, K. Y. Baik, M. Noah, Y.-K. Kwon, J.-O. Lee and S. Hong, *Lab Chip*, 2009, **9**, 2267.
37 W. Yang, K. R. Ratinac, S. P. Ringer, P. Thordarson, J. J. Gooding and F. Braet, *Angew. Chem., Int. Ed.*, 2010, **49**, 2114.
38 J. N. Tey, I. P. M. Wijaya, J. Wei, I. Rodriguez and S. G. Mhaisalkar, *Microfluid. Nanofluid.*, 2010, **9**, 1185.
39 T.-S. Pui, H. G. Sudibya, X. Luan, Q. Zhang, F. Ye, Y. Huang and P. Chen, *Adv. Mater.*, 2010, **22**, 3199.
40 S. Heinze, J. Tersoff, R. Martel, V. Derycke, J. Appenzeller and P. Avouris, *Phys. Rev. Lett.*, 2002, **89**, 106801.
41 A. Javey, J. Guo, D. B. Farmer, Q. Wang, D. W. Wang, R. G. Gordon, M. Lundstrom and H. J. Dai, *Nano Lett.*, 2004, **4**, 447.
42 H. R. Byon and H. C. Choi, *J. Am. Chem. Soc.*, 2006, **128**, 2188.
43 C.-H. Lu, H.-H. Yang, C.-L. Zhu, X. Chen and G.-N. Chen, *Angew. Chem., Int. Ed.*, 2009, **48**, 4785.
44 T. Kuila, S. Bose, P. Khanra, A. K. Mishra, N. H. Kim and J. H. Lee, *Biosens. Bioelectron.*, 2011, **26**, 4637.
45 Y. X. Huang, X. C. Dong, Y. X. Liu, L. J. Li and P. Chen, *J. Mater. Chem.*, 2011, **21**, 12358.
46 Y. Q. Wen, F. B. Y. Li, X. C. Dong, J. Zhang, Q. H. Xiong and P. Chen, *Adv. Healthcare Mater.*, 2013, **2**, 271.
47 Y. X. Huang, X. C. Dong, Y. M. Shi, C. M. Li, L. J. Li and P. Chen, *Nanoscale*, 2010, **2**, 1485.
48 X. T. Zheng, A. Than, A. Ananthanaraya, D. H. Kim and P. Chen, *ACS Nano*, 2013, **7**, 6278.
49 C. X. Guo, S. R. Ng, S. Y. Khoo, X. T. Zheng, P. Chen and C. M. Li, *ACS Nano*, 2012, **6**, 6944.
50 X. W. Wang, X. C. Dong, Y. Q. Wen, C. M. Li, Q. H. Xiong and P. Chen, *Chem. Commun.*, 2012, **48**, 6490.
51 A. H. Castro Neto, F. Guinea, N. M. R. Peres, K. S. Novoselov and A. K. Geim, *Rev. Mod. Phys.*, 2009, **81**, 109.
52 G. Giovannetti, P. A. Khomyakov, G. Brocks, V. M. Karpan, J. van den Brink and P. J. Kelly, *Phys. Rev. Lett.*, 2008, **101**, 026803.
53 F. Xia, V. Perebeinos, Y.-M. Lin, Y. Wu and P. Avouris, *Nat. Nanotechnol.*, 2011, **6**, 179.
54 M. C. Lin, C. J. Chu, L. C. Tsai, H. Y. Lin, C. S. Wu, Y. P. Wu, Y. N. Wu, D. B. Shieh, Y. W. Su and C. D. Chen, *Nano Lett.*, 2007, **7**, 3656.
55 F. Patolsky, G. F. Zheng and C. M. Lieber, *Nat. Protoc.*, 2006, **1**, 1711.
56 Y. Cui and C. M. Lieber, *Science*, 2001, **291**, 851.
57 C.-W. Wang, C.-Y. Pan, H.-C. Wu, P.-Y. Shih, C.-C. Tsai, K.-T. Liao, L.-L. Lu, W.-H. Hsieh, C.-D. Chen and Y.-T. Chen, *Small*, 2007, **3**, 1350.
58 J. Hahm and C. M. Lieber, *Nano Lett.*, 2004, **4**, 51.
59 G. J. Zhang, J. H. Chua, R. E. Chee, A. Agarwal and S. M. Wong, *Biosens. Bioelectron.*, 2009, **24**, 2504.
60 G. F. Zheng, F. Patolsky, Y. Cui, W. U. Wang and C. M. Lieber, *Nat. Biotechnol.*, 2005, **23**, 1294.
61 F. Patolsky, G. F. Zheng, O. Hayden, M. Lakadamyali, X. W. Zhuang and C. M. Lieber, *Proc. Natl. Acad. Sci. U. S. A.*, 2004, **101**, 14017.
62 P.-L. Chiang, T.-C. Chou, T.-H. Wu, C.-C. Li, C.-D. Liao, J.-Y. Lin, M.-H. Tsai, C.-C. Tsai, C.-J. Sun, C.-H. Wang, J.-M. Fang and Y.-T. Chen, *Chem.–Asian J.*, 2012, **7**, 2073.
63 C. M. Lieber, *MRS Bull.*, 2011, **36**, 1052.
64 K.-S. Chang, C.-J. Sun, P.-L. Chiang, A.-C. Chou, M.-C. Lin, C. Liang, H.-H. Hung, Y.-H. Yeh, C.-D. Chen, C.-Y. Pan and Y.-T. Chen, *Biosens. Bioelectron.*, 2012, **31**, 137.
65 F. Patolsky, B. P. Timko, G. Yu, Y. Fang, A. B. Greytak, G. Zheng and C. M. Lieber, *Science*, 2006, **313**, 1100.

66 C.-C. Tsai, C.-C. Yang, P.-Y. Shih, C.-S. Wu, C.-D. Chen, C.-Y. Pan and Y.-T. Chen, *J. Phys. Chem. B*, 2008, **112**, 9165.
67 B.-R. Li, Y.-J. Hsieh, Y.-X. Chen, Y.-T. Chung, C.-Y. Pan and Y.-T. Chen, *J. Am. Chem. Soc.*, 2013, **135**, 16034.
68 B. Tian, T. Cohen-Karni, Q. Qing, X. Duan, P. Xie and C. M. Lieber, *Science*, 2010, **329**, 830.
69 M. Curreli, R. Zhang, F. N. Ishikawa, H.-K. Chang, R. J. Cote, C. Zhou and M. E. Thompson, *Nanotechnology*, 2008, **7**, 651.
70 C.-C. Tsai, P.-L. Chiang, C.-J. Sun, T.-W. Lin, M.-H. Tsai, Y.-C. Chang and Y.-T. Chen, *Nanotechnology*, 2011, **22**, 135503.
71 E. Stern, R. Wagner, F. J. Sigworth, R. Breaker, T. M. Fahmy and M. A. Reed, *Nano Lett.*, 2007, **7**, 3405.
72 G. J. Zhang, G. Zhang, J. H. Chua, R. E. Chee, E. H. Wong, A. Agarwal, K. D. Buddharaju, N. Singh, Z. Q. Gao and N. Balasubramanian, *Nano Lett.*, 2008, **8**, 1066.
73 S.-P. Lin, C.-Y. Pan, K.-C. Tseng, M.-C. Lin, C.-D. Chen, C.-C. Tsai, S.-H. Yu, Y.-C. Sung, T.-W. Lin and Y.-T. Chen, *Nano Today*, 2009, **4**, 235.
74 Y. C. C. Liu, N. Rieben, L. Iversen, B. S. Sorensen, J. Park, J. Nygard and K. L. Martinez, *Nanotechnology*, 2010, **21**, 245105.
75 Y. S. Lo, D. H. Nam, H. M. So, H. Chang, J. J. Kim, Y. H. Kim and J. O. Lee, *ACS Nano*, 2009, **3**, 3649.
76 E. Kang, J.-W. Park, S. J. McClellan, J.-M. Kim, D. P. Holland, G. U. Lee, E. I. Franses, K. Park and D. H. Thompson, *Langmuir*, 2007, **23**, 6281.
77 F. N. Ishikawa, M. Curreli, H.-K. Chang, P.-C. Chen, R. Zhang, R. J. Cote, M. E. Thompson and C. Zhou, *ACS Nano*, 2009, **3**, 3969.
78 C.-J. Chu, C.-S. Yeh, C.-K. Liao, L.-C. Tsai, C.-M. Huang, H.-Y. Lin, J.-J. Shyue, Y.-T. Chen and C.-D. Chen, *Nano Lett.*, 2013, **13**, 2564.
79 X. P. A. Gao, G. F. Zheng and C. M. Lieber, *Nano Lett.*, 2010, **10**, 547.
80 G. F. Zheng, X. P. A. Gao and C. M. Lieber, *Nano Lett.*, 2010, **10**, 3179.
81 T. S. Pui, A. Agarwal, F. Ye, Z. Q. Ton, Y. X. Huang and P. Chen, *Nanoscale*, 2009, **1**, 159.
82 T. S. Pui, A. Agarwal, F. Ye, Y. X. Huang and P. Chen, *Biosens. Bioelectron.*, 2011, **26**, 2746.
83 J. P. Renault, A. Bernard, D. Juncker, B. Michel, H. R. Bosshard and E. Delamarche, *Angew. Chem., Int. Ed.*, 2002, **41**, 2320.
84 N. Naujoks and A. Stemmer, *Microelectron. Eng.*, 2003, **67–68**, 736.
85 R. D. Piner, J. Zhu, F. Xu, S. H. Hong and C. A. Mirkin, *Science*, 1999, **283**, 661.
86 I. Park, Z. Y. Li, A. P. Pisano and R. S. Williams, *Nano Lett.*, 2007, **7**, 3106.
87 M. N. Masood, S. Chen, E. T. Carlen and A. van den Berg, *ACS Appl. Mater. Interfaces*, 2010, **2**, 3422.
88 B.-R. Li, C.-W. Chen, W.-L. Yang, T.-Y. Lin, C.-Y. Pan and Y.-T. Chen, *Biosens. Bioelectron.*, 2013, **45**, 252.
89 H. S. Ro, B. H. Koh, S. O. Jung, H. K. Park, Y. B. Shin, M. G. Kim and B. H. Chung, *Proteomics*, 2006, **6**, 2108.
90 M. Lee, D. K. Kang, H. K. Yang, K. H. Park, S. Y. Choe, C. Kang, S. I. Chang, M. H. Han and I. C. Kang, *Proteomics*, 2006, **6**, 1094.
91 G. Pampalakis and S. O. Kelley, *Analyst*, 2009, **134**, 447.
92 K. Maehashi, K. Matsumoto, Y. Takamura and E. Tamiya, *Electroanalysis*, 2009, **21**, 1285.
93 L. Movileanu, S. Howorka, O. Braha and H. Bayley, *Nat. Biotechnol.*, 2000, **18**, 1091.
94 T.-Y. Lin, B.-R. Li, S.-T. Tsai, C.-W. Chen, C.-H. Chen, Y.-T. Chen and C.-Y. Pan, *Lab Chip*, 2013, **13**, 676.
95 G. J. Zhang, L. Zhang, M. J. Huang, Z. H. H. Luo, G. K. I. Tay, E. J. A. Lim, T. G. Kang and Y. Chen, *Sens. Actuators, B*, 2010, **146**, 138.
96 W. L. C. Rutten, *Annu. Rev. Biomed. Eng.*, 2002, **4**, 407.
97 B. P. Timko, T. Cohen-Karni, G. Yu, Q. Qing, B. Tian and C. M. Lieber, *Nano Lett.*, 2009, **9**, 914.
98 G. Cellot, E. Cilia, S. Cipollone, V. Rancic, A. Sucapane, S. Giordani, L. Gambazzi, H. Markram, M. Grandolfo, D. Scaini, F. Gelain, L. Casalis, M. Prato, M. Giugliano and L. Ballerini, *Nat. Nanotechnol.*, 2009, **4**, 126.
99 T.-S. Pui, A. Agarwal, F. Ye, N. Balasubramanian and P. Chen, *Small*, 2009, **5**, 208.
100 T. Cohen-Karni, D. Casanova, J. F. Cahoon, Q. Qing, D. C. Bell and C. M. Lieber, *Nano Lett.*, 2012, **12**, 2639.
101 N. Misra, J. A. Martinez, S.-C. J. Huang, Y. Wang, P. Stroeve, C. P. Grigoropoulos and A. Noy, *Proc. Natl. Acad. Sci. U. S. A.*, 2009, **106**, 13780.
102 Y. L. Bunimovich, Y. S. Shin, W.-S. Yeo, M. Amori, G. Kwong and J. R. Heath, *J. Am. Chem. Soc.*, 2006, **128**, 16323.
103 X. Duan, Y. Li, N. K. Rajan, D. A. Routenberg, Y. Modis and M. A. Reed, *Nat. Nanotechnol.*, 2012, **7**, 401.
104 M. Zimmermann, E. Delamarche, M. Wolf and P. Hunziker, *Biomed. Microdevices*, 2005, **7**, 99.
105 B. Y. Lee, M. G. Sung, J. Lee, K. Y. Baik, Y.-K. Kwon, M.-S. Lee and S. Hong, *ACS Nano*, 2011, **5**, 4373.
106 H. S. Lee, K. S. Kim, C. J. Kim, S. K. Hahn and M. H. Jo, *Biosens. Bioelectron.*, 2009, **24**, 1801.
107 W. Shen, D. Tian, H. Cui, D. Yang and Z. Bian, *Biosens. Bioelectron.*, 2011, **27**, 18.
108 T. Kong, R. G. Su, B. B. Zhang, Q. Zhang and G. S. Cheng, *Biosens. Bioelectron.*, 2012, **34**, 267.
109 E. Stern, A. Vacic, N. K. Rajan, J. M. Criscione, J. Park, B. R. Ilic, D. J. Mooney, M. A. Reed and T. M. Fahmy, *Nat. Nanotechnol.*, 2010, **5**, 138.
110 J. F. Eschermann, R. Stockmann, M. Hueske, X. T. Vu, S. Ingebrandt and A. Offenhäusser, *Appl. Phys. Lett.*, 2009, **95**, 083703.
111 L. Xu, Z. Jiang, Q. Qing, L. Q. Mai, Q. J. Zhang and C. M. Lieber, *Nano Lett.*, 2013, **13**, 746.
112 B. Z. Tian, P. Xie, T. J. Kempa, D. C. Bell and C. M. Lieber, *Nat. Nanotechnol.*, 2009, **4**, 824.
113 B. D. Almquist and N. A. Melosh, *Proc. Natl. Acad. Sci. U. S. A.*, 2010, **107**, 5815.
114 X. Duan, R. Gao, P. Xie, T. Cohen-Karni, Q. Qing, H. S. Choe, B. Tian, X. Jiang and C. M. Lieber, *Nat. Nanotechnol.*, 2012, **7**, 174.

115 M. L. Seol, J. H. Ahn, J. M. Choi, S. J. Choi and Y. K. Choi, *Nano Lett.*, 2012, **12**, 5603.
116 J. A. Martinez, N. Misra, Y. Wang, P. Stroeve, C. P. Grigoropoulos and A. Noy, *Nano Lett.*, 2009, **9**, 1121.
117 P. K. Ang, M. Jaiswal, C. H. Y. X. Lim, Y. Wang, J. Sankaran, A. Li, C. T. Lim, T. Wohland, Ö. Barbaros and K. P. Loh, *ACS Nano*, 2010, **4**, 7387.
118 S.-C. J. Huang, A. B. Artyukhin, N. Misra, J. A. Martinez, P. A. Stroeve, C. P. Grigoropoulos, J.-W. W. Ju and A. Noy, *Nano Lett.*, 2010, **10**, 1812.
119 K. S. Chang, L. Y. Luo, C. W. Chang, Y. C. Huang, C. Y. Cheng, C. S. Hung, E. W. G. Diau and Y. K. Li, *J. Phys. Chem. B*, 2010, **114**, 4327.
120 K. S. Chang, C. C. Chen, J. T. Sheu and Y. K. Li, *Sens. Actuators, B*, 2009, **138**, 148.